# Super-elastic Continuum Robot for Endoscopic Articulation and Manipulation (SCREAM) 5.0

*Major Qualifying Project*


Submitted By:

Christopher DeMaio, Robotics Engineering

Julia Farnum, Mechanical Engineering

Ananya Gopalan, Robotics Engineering

Jacquelyn Lopez, Robotics Engineering

Project Advisors:

Professor Loris Fichera

Professor Yuxiang Liu





Worcester Polytechnic Institute


August 2022 – May 2023

## Abstract

The objective of this project is to develop a robotic system for in-office laser surgery of the vocal folds. Laryngeal tumors affect approximately 2.5% of the adult population, and office surgery is emerging as a convenient treatment option for these tumors, as opposed to traditional (and more expensive) surgical treatment in the operating room. Unfortunately, not every patient qualifies for office surgery: recent studies indicate that 1 in 3 patients have tumors in locations that physicians cannot reach with the limited instrumentation available in the clinic. To tackle these issues, we explore a new set of needle-thin, highly dexterous robotic instruments, with the overarching goal of amplifying a physician's reach during office procedures. We articulate our proposed instruments using a concentric agonist-antagonist mechanism, which enables tight bending in a small form factor. We propose a novel intuitive control system and an experimental procedure to verify its ability to reduce the difficulty of completing the in-office procedure. Our experiments verify the mechanical capabilities of the device and demonstrate that our device increases the portion of the voice box accessible to the physician during an endoscopic procedure.

## Executive Summary

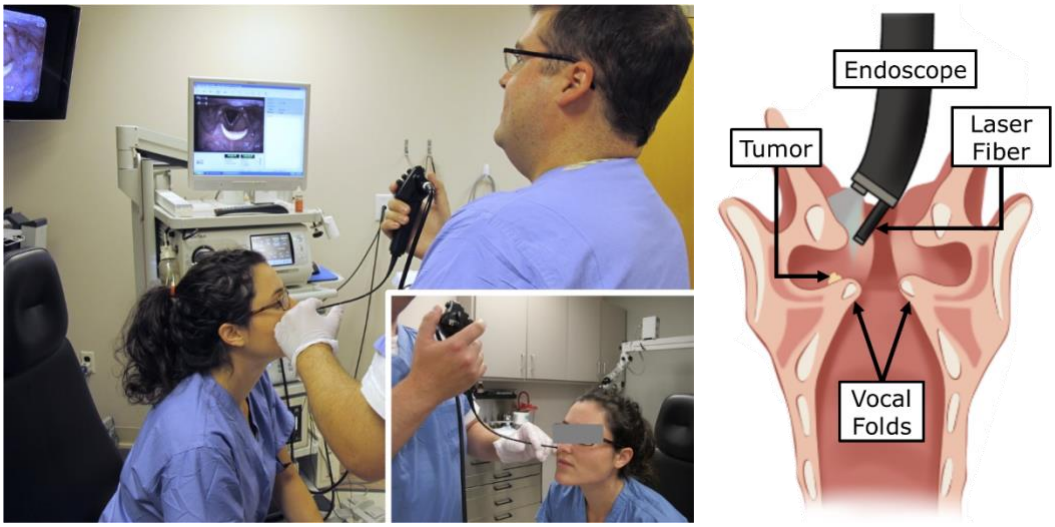


**Figure E.1**: Office-based surgical procedure for the treatment of laryngeal lesions. (Left) A physician passes an endoscope through a patient's nose to access the larynx, using their left hand to hold the endoscope and patient steady and their right hand to steer the endoscope tip. (Right) Cross section of the human larynx. The blue cone represents the endoscope's field of view. To treat the tumor, the physician steers the endoscope so that the laser fiber is pointing at the tumor and the tumor is within the camera's field of view. The physician then fires laser pulses at the tumor to ablate the tumor.

Laryngeal tumors affect 1 in 40 adults worldwide and can cause symptoms including speech discomfort as well as difficult breathing and swallowing [1]. Most patients undergo surgical treatment in the operating room to remove these tumors, but an increasing number of patients are offered the option to receive endoscopic treatment in the clinic instead. Office-based procedures are carried out as shown in Figure 1. These procedures cost less than traditional surgical treatment, require local rather than general anesthesia, and benefit patients with shorter recovery times and lower complication rates [3].

Despite their documented benefits, office-based procedures remain underutilized. This is mainly due to inadequate surgical access: As recent studies have shown [13, 20], clinically available flexible endoscopes do not provide adequate surgical access within the laryngeal cavity, and patients that present with tumors in hard-to-reach locations are ineligible to receive office treatment as a result.

Motivated by these challenges, in this paper we propose a robotic solution to amplify a physician's reach in office-based laryngeal laser surgery. We designed, assembled, and tested the device shown in Figure 2, which consists of an ultra-thin (1.4 mm) flexible chip-on-the-tip endoscope and a steerable optical fiber for laser delivery. These two devices are sufficiently small to permit minimally invasive, trans-nasal deployment into the laryngeal cavity. Articulation is implemented using concentric agonist-antagonist robots (CAARs): an innovative bending mechanism that was recently proposed in the surgical robotics literature [11]–see Figure 3. Briefly, this mechanism is based on the push-pull action of a pair of concentric hypodermic tubes; the tubes are first machined to selectively remove material from their body–thus creating compliant regions–and they are then fixed together at their distal end so that axial translations induce bending in the device. This mechanism enables tight, bi-directional bending in an ultra-thin form factor, which is beneficial for our application: We hope that the enhanced dexterity provided by our

platform will enable physicians to access previously unreachable locations within the laryngeal cavity and ultimately expand the pool of patients eligible for office treatment.

To operate our device, we provide the physician with a wireless user interface. Using a PlayStation 3 controller (Sony Interactive Entertainment, San Mateo, California, USA) as our input device, a physician can complete this procedure without the help of an assistant. The controller allows the physician to deflect, translate, and rotate each continuum robot independently. These degrees of freedom are actuated by the motor unit shown in Figure 4, which consists of two identical cylindrical sections, each of which controls a single continuum robot. We achieve deflection by pushing or pulling on the inner tube of the robot while holding the outer tube fixed. We achieve translation by displacing both the inner and the outer tube by the same amount. Finally, we achieve rotation by turning the cylindrical casing and everything inside it. To transmit forces from the actuation unit to the steel tubes of the continuum robots, we use polyimide tubing reinforced with steel braids (MicroLumen Inc., Oldsmar, FL, USA). This tubing is flexible enough to pass through the bends of the human anatomy yet rigid enough to transmit forces and torques efficiently. Finally, to keep the two robots together, we wrap both CAARs in an access guide made of transparent medical-grade heat shrink. The total area of the access guide is 19.47 $mm^2$, which is smaller than the area taken by a traditional endoscope (19.63 $mm^2$).

We performed experiments to validate our actuation unit's ability to move the CAARs. We determined that the CAAR we used to steer the camera can bend up to 50.3° in the positive direction and 63.3° in the negative direction, with a minimum bending radius of 16 mm. The CAAR we used to steer the laser can bend up to 46.0° in the positive direction and 62.0° in the negative direction, with a minimum banding radius of 13 mm. The laser CAAR has a maximum translation range of 9.05 mm, and the camera CAAR has a maximum translation range of 9.60 mm. Both CAARs can rotate without limit in both directions.

Our proposed device represents a radical departure from the solutions offered by previous SCREAM projects. SCREAM 1 and SCREAM 2 explored the viability of continuum robots for trans-nasal laser surgery [7, 8]. SCREAM 3 and SCREAM 4 developed design iterations for an attachment to existing endoscopes [4, 9]. Instead of developing another handheld attachment, we approached the clinical problem from a new perspective. While our device is not suitable for clinical trials, it has overcome key problems faced by previous groups, such as the coupling of the motion of the optical fiber and the camera.

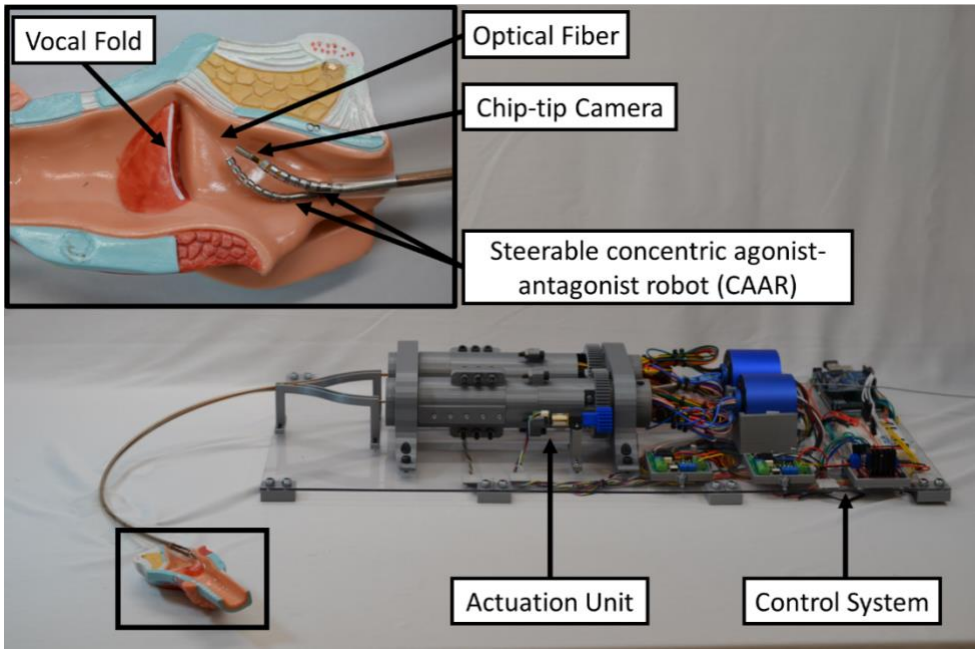


**Figure E.2**: Proposed robotic surgical device for office-based surgery. with key components and human anatomy labeled. We use a pair of hollow continuum robots to steer the optical fiber and the chip-tip camera in the larynx. Our control system enables a physician to complete the procedure wirelessly without the help of an assistant. The actuation unit enables independent control of three degrees of freedom for each robot.

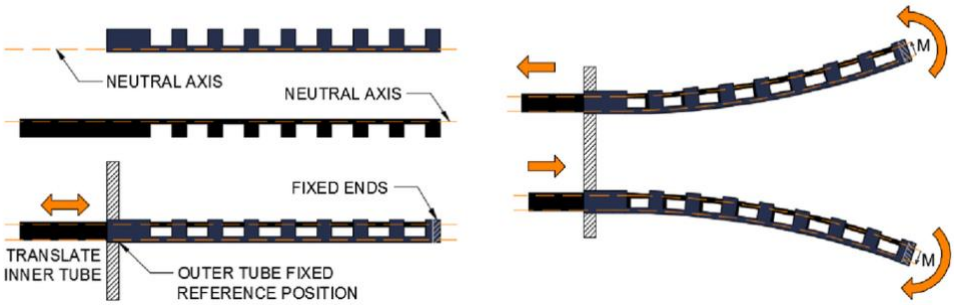


**Figure E.3**: Concentric agonist-antagonist robots deflect when the inner tube translates and the outer tube remains fixed. Reproduced from [11].

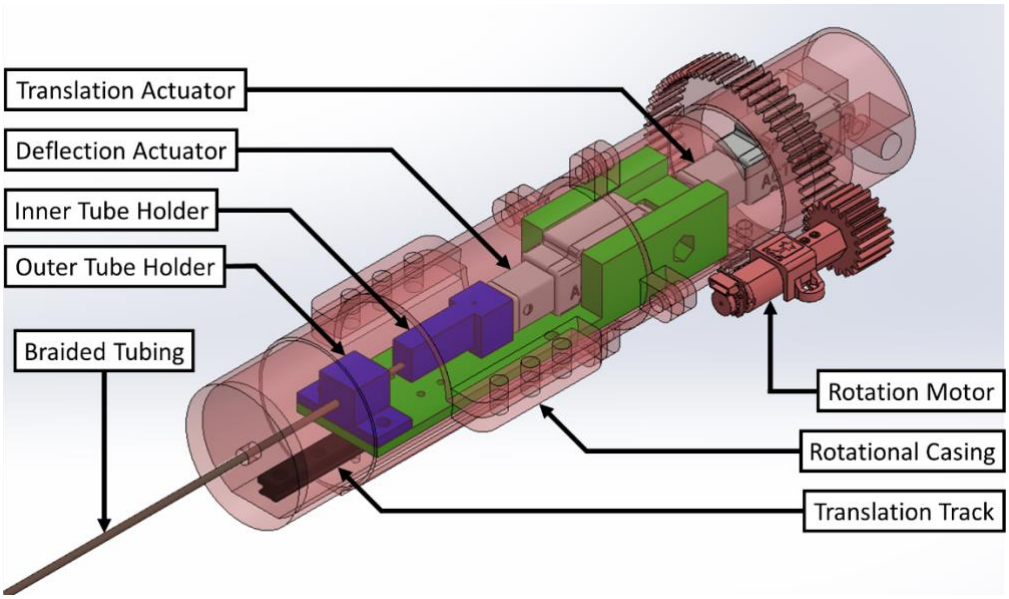


**Figure E.4**: Schematic of the actuation unit for a CAAR manipulator, with key components labeled.

## Acknowledgments

This Major Qualifying Project was supported by the Worcester Polytechnic Institute (WPI) and the Cognitive Medical Technology Laboratory. We appreciate the support they have given us throughout the project.

We are grateful to WPI and to the National Institute on Deafness and Communication Disorders (NIDCD) (award no. R15DC018667) for providing us with the funds we used to complete this project.

We would like to thank our advisors, Professor Loris Fichera and Professor Yuxiang Liu, for the guidance and advice they have given us and for their support during the highs and lows of this project.

We would like to thank Alex Chiluisa and Nicholas Pacheco for their mentorship and for the help they provided while we designed and tested our device.

We would like to thank Dr. Thomas Carroll for his continued support of this project and for his expert opinion as a laryngologist.

We would like to thank Kalina Bonofiglio for her assistance in manufacturing components for our device.

## Authorship

| Section | Author |
|---|---|
| **Abstract** | **CD** |
| **Executive Summary** | **CD** |
| **1 Introduction** | **CD** |
| 1.1 Background | CD |
| 1.2 Paper Outline | CD |
| **2 Design and Fabrication** | **CD JF AG JL** |
| 2.1 Gathering of Requirements | CD |
| 2.2 Steerable Sheaths | CD JF AG |
| 2.2.1 CAAR Kinematics | CD AG |
| 2.2.2 Kinematic Simulations | AG |
| 2.2.3 CAAR Design Process | JF |
| 2.3 Endcaps | JF |
| 2.4 Transferring Motion | CD |
| 2.4.1 Braided Tubes | CD |
| 2.4.2 Heat Shrink | CD |
| 2.5 Actuation Unit | CD |
| 2.5.1 Deflection | CD |
| 2.5.2 Translation | CD |
| 2.5.3 Rotation | CD |
| 2.6 Control System | JL |
| **3 Experimentation and Validation** | **CD** |
| 3.1 Setup | CD |
| 3.2 Deflection | CD |
| 3.2 Translation | CD |
| 3.3 Rotation | CD |
| **4 Discussion and Future Work** | **JF** |
| 4.1 Future Work | JF |
| 4.2 Conclusion | JF |
| **Appendix A: Machining Process for the Laser and Camera CAARs** | **JF** |
| **Appendix B: Machining Process for the Laser and Camera Endcaps** | **JF** |
| **Appendix C: Physician User Study** | **AG JL** |
| **Appendix D: Control System Wiring Schematic** | **CD** |

## Table of Contents

## List of Tables

## List of Figures

# 1 Introduction

## 1.1 Background

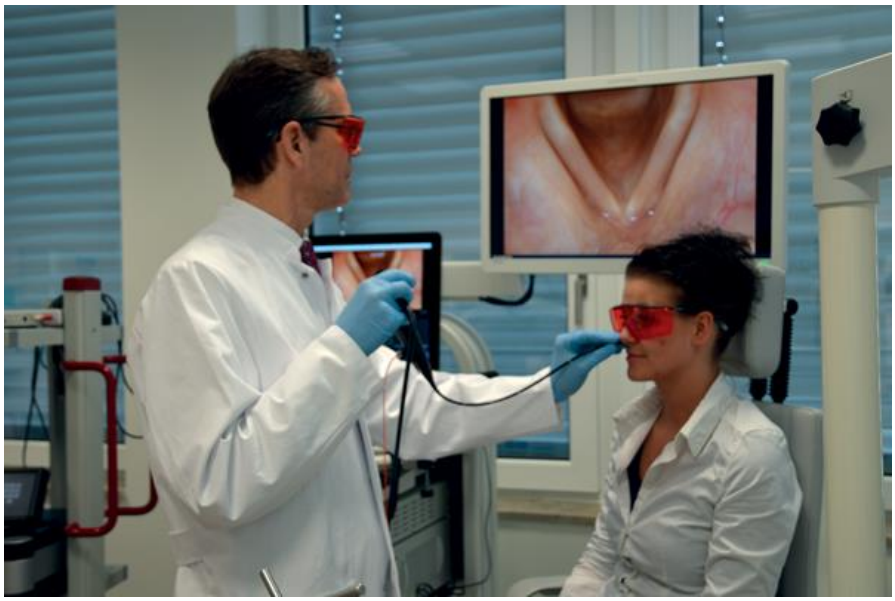

**Figure 1.1**: Office-based procedure for treating laryngeal lesions. The physician uses their left hand to keep the patient and the device stable while steering the device and activating the laser with their right hand. Reproduced from [15].

Laryngeal lesions affect approximately 1 in 40 people worldwide and can cause a variety of symptoms, including speech discomfort, as well as difficult breathing and swallowing [1]. Physicians traditionally remove these lesions in the operating room under general anesthesia [2]. Because surgical treatment can be expensive and can cause complications, in recent years, researchers have explored ways to treat laryngeal tumors in the clinic, as an outpatient procedure [3]. Office-based laryngeal procedures are performed as shown in Figure 1.1. The physician first inserts a flexible endoscope through the patient's nose and into their throat. The endoscope includes a camera that allows the physician to inspect the target tissue and an optical fiber that the physician uses to deliver laser pulses and thus thermally necrotize diseased tissue [4]. Office-based procedures offer many benefits, including lower costs ($5000 less than traditional surgical treatment) and shorter recovery time [5, 6]. Furthermore, a physician can complete the procedure in a matter of minutes without general anesthesia [2].

Despite the advantages of in-office procedures, certain barriers exist that prevent the approach from being widely adopted. Commercially available optical fibers provide physicians with no means of direct articulation; as a result, physicians can only steer the optical fiber by bending the distal tip of the endoscope. This prevents physicians from accessing large portions of the larynx [13]. Patients with tumors in inaccessible locations cannot receive in-office treatment and must instead undergo the traditional procedure (see Figure 1.2). Additionally, because the physician cannot control the laser without moving the camera, the procedure can be disorienting [21]. This may cause the physician to fail to thoroughly remove the tumor, leaving the patient in need of an additional procedure.

Motivated by these challenges, in this paper we propose a robotic solution to amplify a physician's reach in office-based laryngeal laser surgery. We designed, assembled, and tested the device shown in Figure

1.3, which consists of an ultra-thin (1.4 mm) flexible chip-on-the-tip endoscope and a steerable optical fiber for laser delivery. These two devices are sufficiently small to permit minimally invasive, trans-nasal deployment into the laryngeal cavity. Articulation is implemented using an innovative bending mechanism that was recently proposed in the surgical robotics literature [11]–see Figure 1.4. Briefly, this mechanism is based on the push-pull action of a pair of concentric hypodermic tubes; the tubes are first machined to selectively remove material from their body–thus creating compliant regions–and they are then fixed together at their distal end, so that axial translations induce bending in the device. This mechanism enables tight, bi-directional bending in an ultra-thin form factor, which is beneficial for our application: We hope that the enhanced dexterity provided by our platform will enable physicians to access previously unreachable locations within the laryngeal cavity and ultimately expand the pool of patients eligible for office treatment.

We built upon the work of four prior MQP teams [4, 7, 8, 9], who developed an attachment to a traditional endoscope that allowed physicians to steer the optical fiber. This project explores a radical new concept: rather than developing an attachment to existing handheld endoscopes, we created a novel device that does not conform to the existing surgical workflow. Our optical fiber and chip-tip camera are smaller than the ones used by previous devices. We decoupled the motion of the optical fiber and the camera, allowing physicians, for the first time, to move these instruments independently of each other. Our continuum robots allow for active bidirectional bending, and they do not rely on a tendon. We present the physician with a user interface based upon a wireless gaming controller rather than a traditional surgical device.

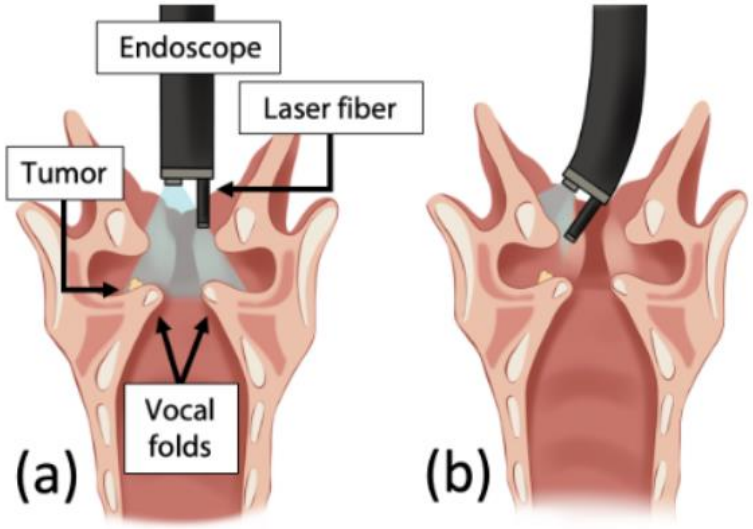


**Figure 1.2**: Frontal cut of the larynx. (b) Tumors often develop in regions that traditional endoscopes cannot reach or in regions where the laser fiber obstructs the camera. Reproduced from [8].

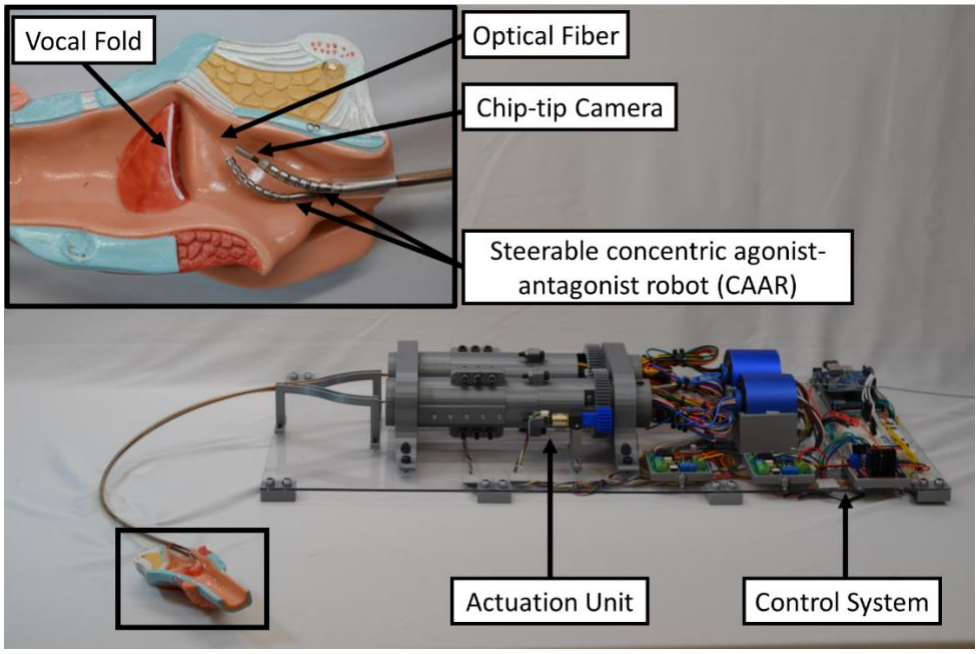


**Figure 1.3**: Robotic surgical device with key components and human anatomy labeled. The two cylindrical casings and the attached motors comprise the actuation unit, which enables the physician to rotate, translate, and bend a pair of continuum robots. The chip-tip camera passes through the hollow lumen of one continuum robot, while the laser fiber passes through the hollow lumen of a second continuum robot. The control system contains the electronics necessary to control the actuators and communicate with the wireless controller.

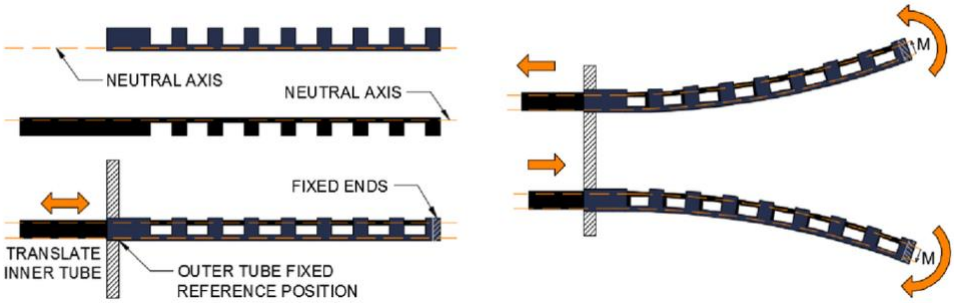


**Figure 1.4**: Concentric agonist-antagonist robots deflect when the inner tube translates and the outer tube remains fixed. Reproduced from [11].

### 1.2 Paper Outline

The contents of this paper are as follows: **Design and Fabrication** describes our functional and non-functional requirements, prior work done on the project, and our design solutions; **Experimentation and Validation** describes the tests we performed to verify the efficacy of our solution; and **Discussion and Future Work** describes our project's limitations, our suggestions for future work, and the broader impacts of our project.

## 2 Design and Fabrication

In this chapter, we present the requirements for our robotic system. We discuss our designs, including how those designs satisfy the system requirements. Our proposed device consists of an ultra-thin (1.4 mm) flexible chip-on-the-tip endoscope and a steerable optical fiber for laser delivery. These two devices are sufficiently small to permit minimally invasive, trans-nasal deployment into the laryngeal cavity. We implement articulation using CAARs, which enable tight, bi-directional bending in an ultra-thin form factor. To operate our device, we provide the physician with a wireless user interface that allows the physician to control three independent degrees of freedom for each CAAR. These degrees of freedom—deflection, translation, and rotation, are actuated by our motor unit, which is connected to the CAARs by reinforced polyimide tubing. The CAARs are passed through an elliptical access guide with a major axis of length 5.7 mm and minor axis of length 4.35 mm.

### 2.1 Design Specifications

We developed the following set of system requirements (SRs) that our novel device needed to satisfy:

**SR1.** The access guide must not exceed 5 mm in total diameter.

Our device will reach the larynx by first passing through the patient's nose. To ensure that our device will fit through the nose and will not cause unnecessary discomfort to the patient, it should be no larger than the endoscopes traditionally used for in-office procedures.

**SR2.** The camera and optical fiber must move independently, and each must have three independently controllable degrees of freedom.

Commercially available endoscopes fail to provide physicians with a means of moving the camera without also moving the optical fiber. Our device must provide the physician with the maximum possible control over the two tools so that the physician can treat greater portions of the larynx.

**SR3.** The device must provide the physician with a simple, intuitive control system that requires no more than one operator.

The current in-office procedure requires a high physician skill level, and it forces physicians to stretch their hands into uncomfortable positions. Our device should allow physicians to complete the procedure without discomfort. Additionally, implementing a control system that reduces the procedure's difficulty will allow a greater number of physicians to learn the procedure and subsequently increase global access to laryngeal treatment.

### 2.2 Steerable Sheaths

Bending in our device is implemented with a concentric agonist-antagonist robot (CAAR) to actuate the laser fiber and another CAAR to actuate the camera. A CAAR consists of two notched-tube wrists rigidly attached at their distal ends, with their notches facing in opposite directions [11]. To actuate the wrist, the outer tube is held still, and the inner tube is translated forward or backward (see Figure 2.1). Because a CAAR includes two notched-tube wrists, it does not require a tendon for actuation, and it is capable of bidirectional bending. Additionally, because the wrist provides active bending in both directions, we do not rely on the elasticity of the wrist itself to return the wrist to an unbent state after it has been bent.

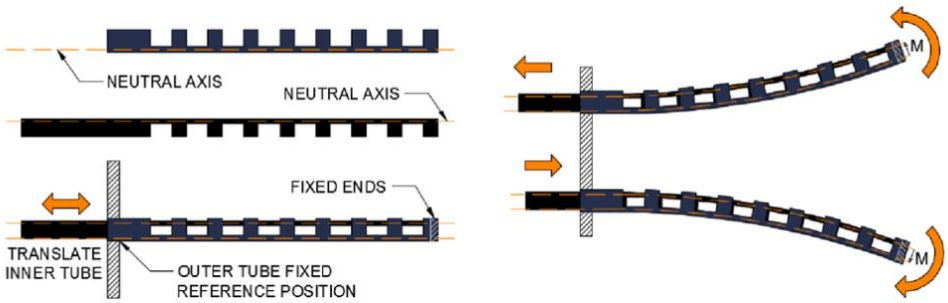


**Figure 2.1:** Concentric agonist-antagonist robots deflect when the inner tube translates and the outer tube remains fixed. Reproduced from [11].

### *2.2.1 CAAR Kinematics*

To design and control continuum robots, we must understand how an actuation input affects a continuum robot's configuration. The forward kinematics of the continuum robot determines the robot's position based on a given set of actuator inputs.

Traditionally, engineers model kinematic chains using the Denavit-Hartenberg (DH) convention as described in [19]. However, this method cannot be applied to continuum robots because continuum robots, by definition, do not contain discrete joints. Therefore, we use the kinematic approach developed by Webster et al [12].

As Figure 2.2 shows, Webster et al [12] separate the kinematics problem into two parts: robot-independent mapping, in which the arc parameters are mapped to the robot's task space pose, and robot-specific mapping, in which the actuation inputs are mapped to the arc parameters. The arc parameters are $\kappa$, which represents the robot's curvature; $\phi$, which represents the robot's rotation, and $s$, which represents the robot's arc length (see Figure 2.3). To simplify the calculations, we assume that each of the robot's notches bends with a constant curvature.

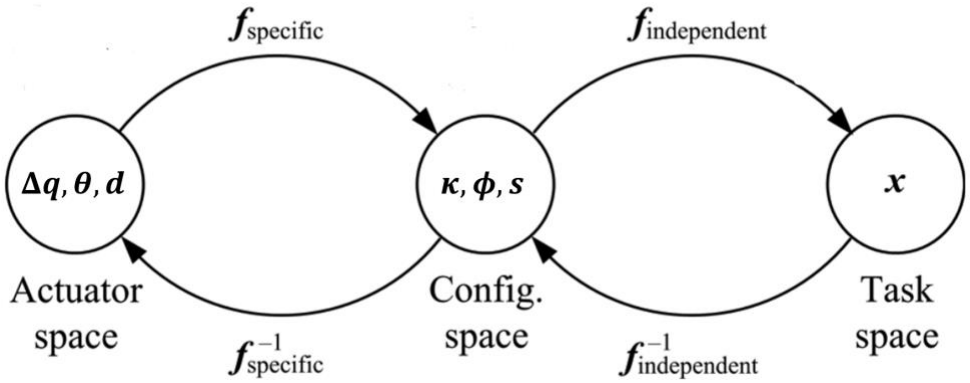


**Figure 2.2**: Robot-specific mapping determines how actuation inputs $\Delta q$ (displacement of the CAAR's inner tube), $\theta$ (rotation of the CAAR), and $d$ (translation of the CAAR) map to the arc parameters $\kappa$ (curvature), $\phi$ (rotation), and $s$ (arc length). Robot-independent mapping determines the robot's pose in task space based on the arc parameters. Adapted from [12].

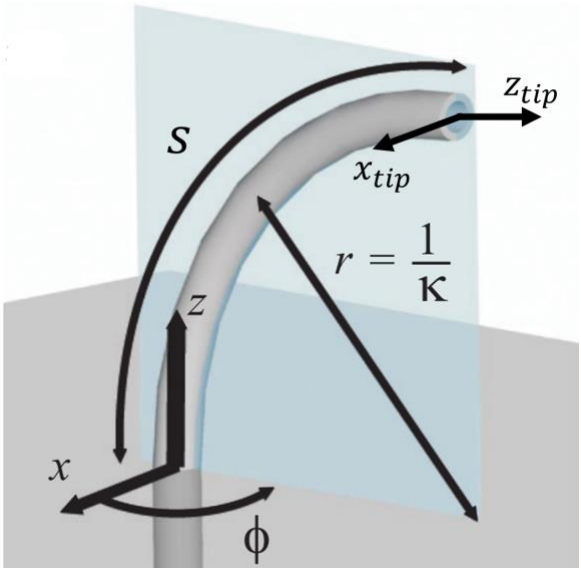


**Figure 2.3**: Arc parameters for a continuum robot with constant curvature. κ represents the robot's curvature. φ represents the angle of robot rotation required to make the y axis at the base parallel to the y axis at the tip (assuming a right-handed coordinate frame). $s$ represents the robot's arc length. Adapted from [12].

#### 2.2.1.1 Robot-Independent Mapping

We first map the arc parameters to the robot's pose in task space. According to Webster et al [12], the transformation from the base of a notched section to the tip of that notched section can be represented by a pair of twists $\xi_{rot}$ and $\xi_{inp}$. $\xi_{rot}$ represents the rotation about the z axis needed to align the y axis of the base frame and the y axis of the tip frame:

(2.1) $$\xi_{rot} = \begin{bmatrix} \vartheta_{rot} \\ \omega_{rot} \end{bmatrix} = [0 \quad 0 \quad 0 \quad 0 \quad 0 \quad 1]^T$$

$\xi_{inp}$ represents the transformation in the $x - z$ plane needed to bring the frame from the base of the notch to the tip:

(2.2) $$\xi_{inp} = \begin{bmatrix} \vartheta_{inp} \\ \omega_{inp} \end{bmatrix} = [0 \quad 0 \quad 1 \quad 0 \quad \kappa \quad 0]^T$$

We map these twists to the Lie algebra $\mathfrak{se}(3)$ of the special Euclidean group $SE(3)$, and we denote this mapping with the ˆ operator.

(2.3) $$\hat{\xi}_{rot} = \begin{bmatrix} \widehat{\omega}_{rot} & \vartheta_{rot} \\ 0_{1x3} & 0 \end{bmatrix} = \begin{bmatrix} 0 & -1 & 0 & 0 \\ 1 & 0 & 0 & 0 \\ 0 & 0 & 0 & 0 \\ 0 & 0 & 0 & 0 \end{bmatrix}$$

(2.4) $$\hat{\xi}_{inp} = \begin{bmatrix} \widehat{\omega}_{inp} & \vartheta_{inp} \\ 0_{1x3} & 0 \end{bmatrix} = \begin{bmatrix} 0 & 0 & \kappa & 0 \\ 0 & 0 & 0 & 0 \\ -\kappa & 0 & 0 & 1 \\ 0 & 0 & 0 & 0 \end{bmatrix}$$

We use the product of exponentials to generate the 4x4 homogeneous transformation matrix associated with a single notched section of the robot:

(2.5) $$T_{notch} = e^{\hat{\xi}_{rot}\phi} e^{\hat{\xi}_{inpl}}$$

(2.6) $$T_{notch} = \begin{bmatrix} \cos\phi\cos(\kappa s) & -\sin\phi & \cos\phi\sin(\kappa s) & \frac{(\cos\phi)(1-\cos(\kappa s))}{\kappa} \\ \sin\phi\cos(\kappa s) & \cos\phi & \sin\phi\sin(\kappa s) & \frac{(\sin\phi)(1-\cos(\kappa s))}{\kappa} \\ -\sin(\kappa s) & 0 & \cos(\kappa s) & \frac{\sin(\kappa s)}{\kappa} \\ 0 & 0 & 0 & 1 \end{bmatrix}$$

Assuming that uncut sections of the tube do not bend, we can derive the transformation between the tip of one notch and the base of the next notch by taking the limit of $T$ as $\kappa$ approaches 0:

(2.7) $$T_{uncut} = \lim_{\kappa \to 0} T_{notch}$$

Finally, to calculate the transformation between the base and the tip of a notched tube, we post-multiply the homogeneous transformation matrices for each section of the tube:

(2.8) $$T = \prod_{i=1}^{n} T_{notch,i} T_{uncut,i}$$

where $n$ is the number of notches in the tube.

#### 2.2.1.2 Robot-Specific Mapping

To map the actuation inputs to the arc parameters, we must first calculate the location of the neutral bending plane of each tube in the CAAR; as shown in Figure 2.4, the neutral bending plane is the portion of the tube that neither compresses nor tenses when the tube is bent [22]. To find the distance $\bar{y}$ between the neutral bending plane and the central axis of the tube, we use the following equations, with variables as illustrated in Figure 2.5 [22]:

(2.9) $$\bar{y} = \frac{\bar{y}_0 A_0 - \bar{y}_i A_i}{A_0 - A_i}$$

(2.10) $$A_0 = \frac{{r_0}^2(\varphi_0 - \sin(\varphi_0))}{2} \quad A_i = \frac{{r_i}^2(\varphi_i - \sin(\varphi_i))}{2}$$

(2.11) $$\bar{y}_0 = \frac{4 r_0 sin^3(\frac{1}{2}\varphi_0)}{3(\varphi_0 - \sin(\varphi_0))} \quad \bar{y}_i = \frac{4 r_i sin^3(\frac{1}{2}\varphi_i)}{3(\varphi_i - \sin(\varphi_i))}$$

(2.12) $$\varphi_0 = 2\arccos\left(\frac{g - r_0}{r_0}\right) \quad \varphi_i = 2\arccos\left(\frac{g - r_o}{r_i}\right)$$

Having solved for the locations of the neutral bending planes of both tubes of the CAAR, we can calculate the total bending angle $\gamma$ using the following equation [11]:

(2.13) $$\gamma = \tau(\overline{y_1} + \overline{y_2})^{-1}$$

where $\overline{y_1}$ is the location of the neutral bending plane of the outer tube, and $\overline{y_2}$ is the location of the neutral bending plane of the inner tube.

We assume that the uncut notches do not bend and that each notch bends at the same angle. Therefore, the total bending angle $\gamma$ can be distributed evenly across all notches [22]:

(2.14) $$\gamma_j = \frac{\gamma}{n}$$

We can then calculate the arc length and curvature of each notch $j$ [11]:

(2.15) $$s_j = h - \bar{y}_1\gamma_j$$

(2.16) $$\kappa_j = \frac{\gamma_j}{s_j}$$

Equations 2.6-2.8 can then be used to convert these curvature and arc length values into the robot's task space pose. To handle any rotation $\theta$ or translation $d$ applied to the CAAR, we can pre-multiply the product in Equation 2.6 by an extra transformation matrix with $\kappa = 0$ and $s = d$.

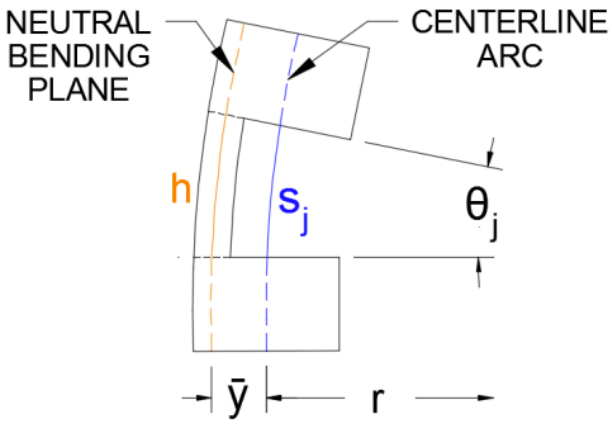


**Figure 2.4**: Cutting notches in the tube shifts the neutral bending plane away from the central axis of the tube. Adapted from [11].

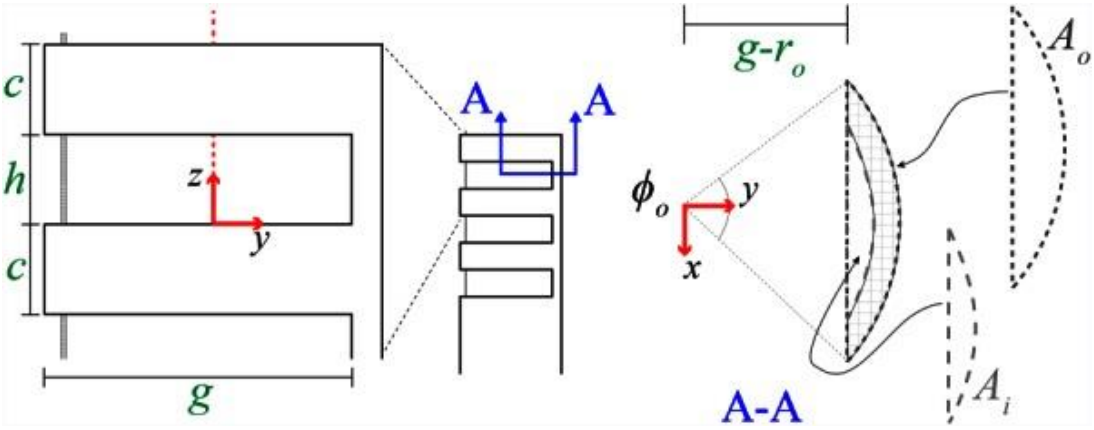


**Figure 2.5**: Illustration of variables needed to calculate the location of the neutral bending plane of a notched tube robot. Adapted from [22].

### *2.2.2 Kinematic Simulations*

A steerable endoscope with a CAAR end effector was simulated in a virtual environment to test the viability and reachability of the device. The purpose of this study is to get an early sense of whether CAARs provide more coverage compared to the current state of the art and to previous SCREAM teams. The simulation used a three-dimensional human larynx model generated by micro-computerized tomography scans, published by Bailly et al [24] An X-ray microtomography with voxel sizes between 25 and 45 µm was used to attain these images. Each larynx model was prepared by compiling the images into three-dimensional stereolithography (STL) models with a custom MATLAB (The MathWorks, Natick, MA, USA) script. To reduce the computational cost of these simulations, the STL models were post-processed with the Quadric Edge Collapse Decimation filter in MeshLab [14]. A MATLAB script was used to control and simulate the endoscope's reachable space. The endoscope simulated in this study is the Pentax VNL-1570STK14, modified to include a CAAR end effector. This flexible nasal laryngoscope has a working channel of 2mm and a diameter of 4.9mm. This larynx model is shown in Figure 2.6.

The endoscope's camera is positioned above the right vocal fold of the larynx and the laser fiber is positioned on the left vocal fold. The device can be translated, bent, and rotated. The endoscope bends at a constant curvature between -120° and 120° and rotates between -100° and 100°. The simulation tests 10,000 points of endoscope configurations using a sample-based motion planning algorithm, Rapidly Exploring Random Trees (RRT). RRT is a motion planning algorithm that builds a search tree incrementally from samples randomly drawn from a given state space. The tree eventually spans the search space and connects the start state to the goal state [23]. We use 10,000 points here because many points are necessary to build a map of reachable tissue. In each of these configuration points, a ray-casting algorithm is run to simulate the application of laser light. This algorithm generates 1,000 virtual rays from the fiber tip in a cone that mimics the laser beam. The Moller-Trumbore ray-triangle Intersection algorithm is applied to each ray to detect what faces of the STL larynx model are visible in a direct line of sight. STL faces that are located more than 3 mm away from the tip of the laser fiber would not be irradiated with a sufficient power density. This is due to the divergence of the laser beam, resulting in these points being marked as unreachable. The total reachable surface area of a traditional endoscope within the larynx is 11.29 $cm^2$, while the total reachable surface area of the endoscope with an additional CAAR is 19.71 $cm^2$. The comparison between the visibility of a traditional endoscope and our device is shown in Figure 2.7.

The models show an increase in reachable surface area with the use of a CAAR, demonstrating the concept's clinical utility.

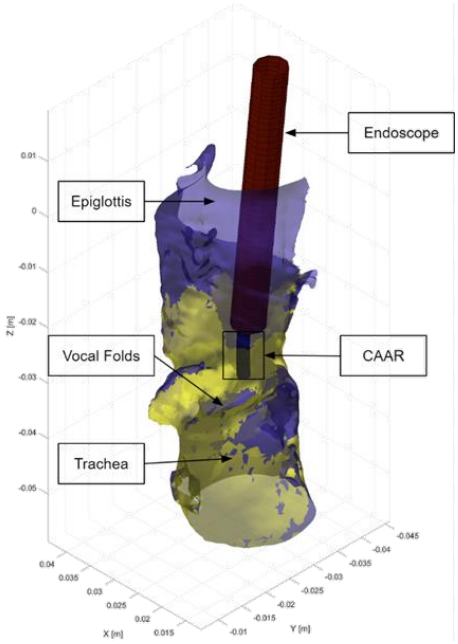


**Figure 2.6**: Larynx and endoscope model used for MATLAB simulations.

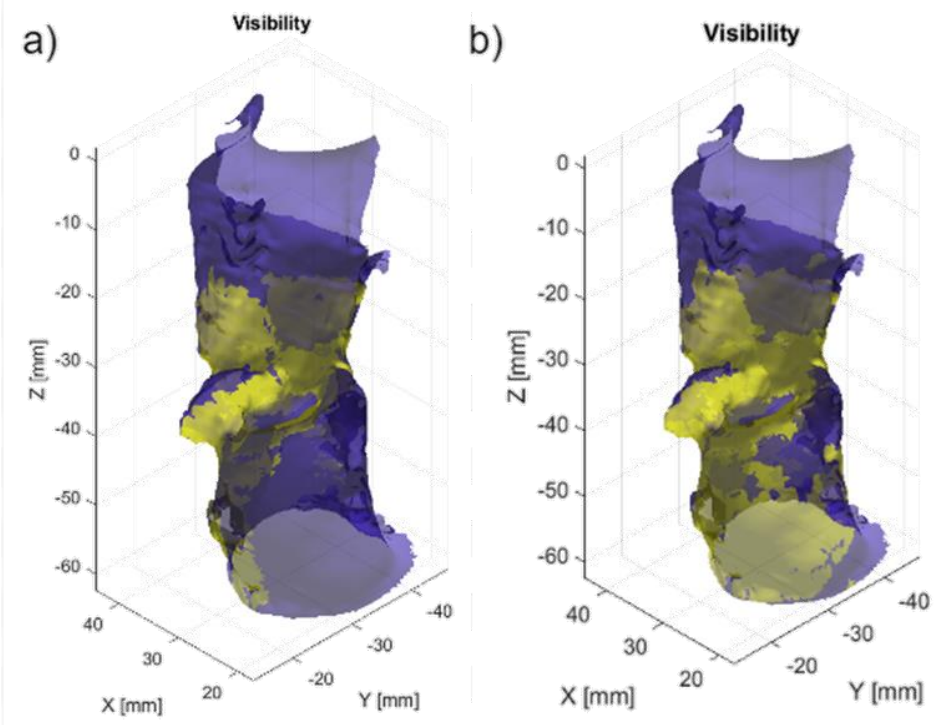


**Figure 2.7**: Three-dimensional model of a) a traditional endoscope reachable surface area and b) the CAAR reachable surface area within the Larynx model. Tissue shown in yellow is considered treatable, while tissue shown in purple is considered untreatable.

### *2.2.3 CAAR Design Process*

During the design process for the laser and camera CAARs, we considered multiple design points to optimize the CAARs. The first design point was the amount of strain that the CAARs would undergo when they were actuated. For our prototype, we used stainless steel for the tubing of the CAAR. However, because Nitinol would most likely be used in a surgical procedure, we based our design on the properties of Nitinol. Nitinol has super elastic properties that allow it to recover from strains up to 8%; above 8% strain, it undergoes plastic deformation. To avoid plastic deformation, we set the maximum allowable strain for our CAARs at 8%. Through simulations, we found an optimized laser CAAR design with a maximum of 6% strain and a camera CAAR design with a maximum of 6.7% strain.

The next design point that we considered was the bending radius of the CAARs. There were multiple considerations that we had for the bending radius of the CAARs. The first was the size of the larynx. The diameter of the larynx is about 40 mm, varying slightly depending on the person [18]. The next consideration was that we wanted to have a tight enough bending radius that provided us with excellent steerability, but not so tight that the bending motion would damage the laser fiber or the camera. We decided to set the maximum bending radius for the CAARs to be 20 mm. The final design of the laser CAAR had a bending radius of 13 mm and the camera CAAR had a bending radius of 16 mm.

The parameters we chose for the laser CAAR and camera CAAR are shown in Tables 1 and 2, respectively. An illustration of these parameters is shown in Figure 2.8. For information about the CAAR manufacturing process, please refer to Appendix A.

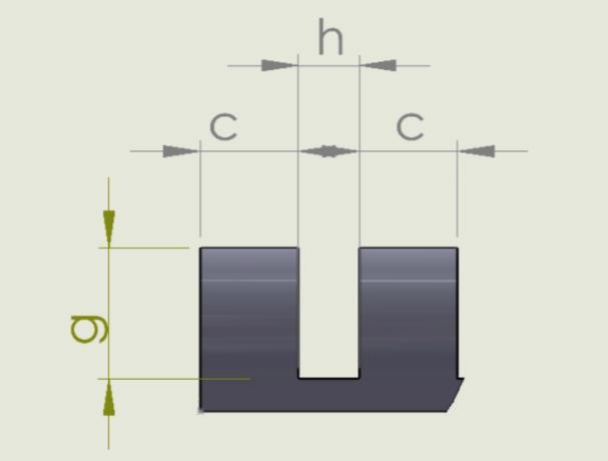


**Figure 2.8**: Design parameters of a notched tube.

**Table 1**: Dimensions of the inner and outer stainless-steel tubing for the laser CAAR.

| | **Inner** | **Outer** |
|---|---|---|
| Outer Diameter (mm) | 1.270 | 1.980 |
| Notch Height, *h* (mm) | 1.000 | 1.000 |
| Notch Depth, *g* (mm) | 1.080 | 1.683 |
| Uncut Height, *c* (mm) | 1.188 | 1.188 |
| Number of Notches, *n* | 8 | 8 |

**Table 2**: Dimensions of the inner and outer stainless-steel tubing for the camera CAAR.

| | Inner | Outer |
|---|---|---|
| Outer Diameter (mm) | 1.980 | 2.413 |
| Notch Height, *h* (mm) | 1.000 | 1.000 |
| Notch Depth, *g* (mm) | 1.683 | 2.051 |
| Uncut Height, *c* (mm) | 1.448 | 1.448 |
| Number of Notches, *n* | 8 | 8 |

### 2.3 Endcaps

The endcaps are used to hold the inner tube and outer tube of a CAAR together. It is important that the inner tube and outer tube are held fixed because this is what allows the CAAR to bend. With the ends fixed and the outer tube held still, as the inner tube is translated forward, the CAAR bends in one direction. As the inner tube is translated backwards, the CAAR bends in the opposite direction.

Each endcap consists of a circular aluminum disk with a ridge that connects the inner and outer tubes as well as a drilled hole to allow the laser (0.22 mm in diameter) or camera (1.44 mm in diameter) to pass through. The geometry of the laser endcap and camera endcap can be seen in Figure 2.9. The dimensions of the laser and camera CAARs can be found in Table 3. For information about the endcap manufacturing process, please refer to Appendix B.

**Table 33**: Dimensions of the endcaps used to construct the laser and camera CAARs.

| | Laser | Camera |
|---|---|---|
| **Outer Diameter (mm)** | 1.98 | 2.41 |
| **Ridge Outer Diameter (mm)** | 1.60 | 2.16 |
| **Ridge Inner Diameter (mm)** | 1.27 | 1.98 |
| **Hole Diameter (mm)** | 0.22 | 1.44 |
| **Height (mm)** | 1.20 | 1.20 |

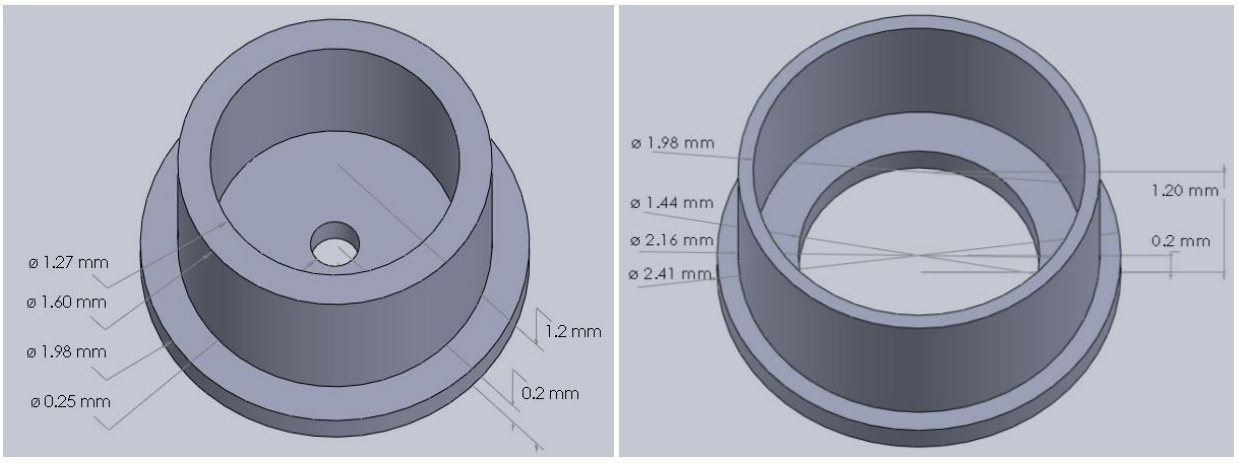


**Figure 2.9**: Left: Laser endcap with dimensions. Right: Camera endcap with dimensions. Dimensions are shown in millimeters.

## 2.4 Transferring Motion

### *2.4.1 Braided Tubes*

Previous SCREAM teams used a spring coil to transfer motion from the actuation unit to the steerable wrist [4]. Because our device includes four notched-tube wrists, we cannot transfer motion to them via spring coils while maintaining a total access guide diameter under 5 mm (SR 1). For that reason, we used polyimide tubing reinforced with stainless-steel braids. This braided tubing is flexible enough to pass through a patient's nose and throat while being strong enough to transfer the required forces without kinking. The tubing can be produced with a wall thickness below 100 µm; the tubing's low profile helps satisfy SR 1.

Table 4 lists the dimensions of the braided tubes we used in our device. All tubing was sourced from MicroLumen, Inc. (Oldsmar, FL, USA). As shown in Figure 2.10, each braided tube was attached to the base of the corresponding notched tube by applying superglue to the exterior of the notched tube's base and inserting the notched tube into the braided tube. The braided tubes were attached to the actuation unit by applying superglue to the exterior of the braided tube and inserting the braided tube into either the CAAR Inner Tube Holder or CAAR Outer Tube Holder (see Figure 2.11).

**Table 44**: Braided Tubing Dimensions.

| Corresponding Notched Tube | | Notched Tube Outer Diameter | Braided Tube Inner Diameter | Braided Tube Outer Diameter | Braided Tubing Length |
|---|---|---|---|---|---|
| Laser CAAR | Inner Tube | 1.27 mm | 1.351 mm | 1.742 mm | TBD |
| | Outer Tube | 1.98 mm | 2.103 mm | 2.306 mm | TBD |
| Camera CAAR | Inner Tube | 1.98 mm | 2.103 mm | 2.306 mm | TBD |
| | Outer Tube | 2.413 mm | 2.540 mm | 2.799 mm | TBD |

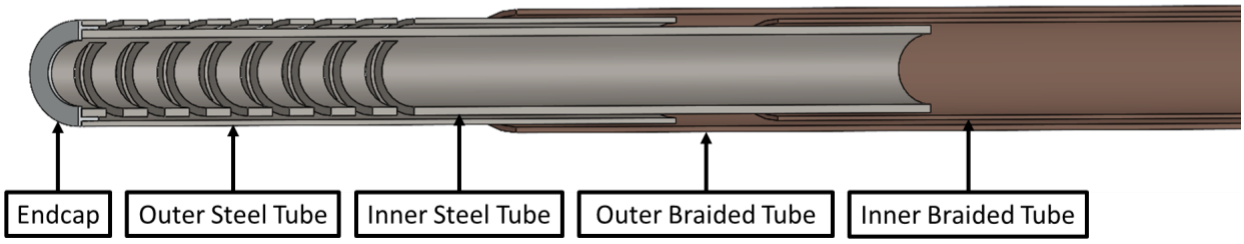


**Figure 2.10**: Cross-sectional view of camera CAAR and attached braided tubes.

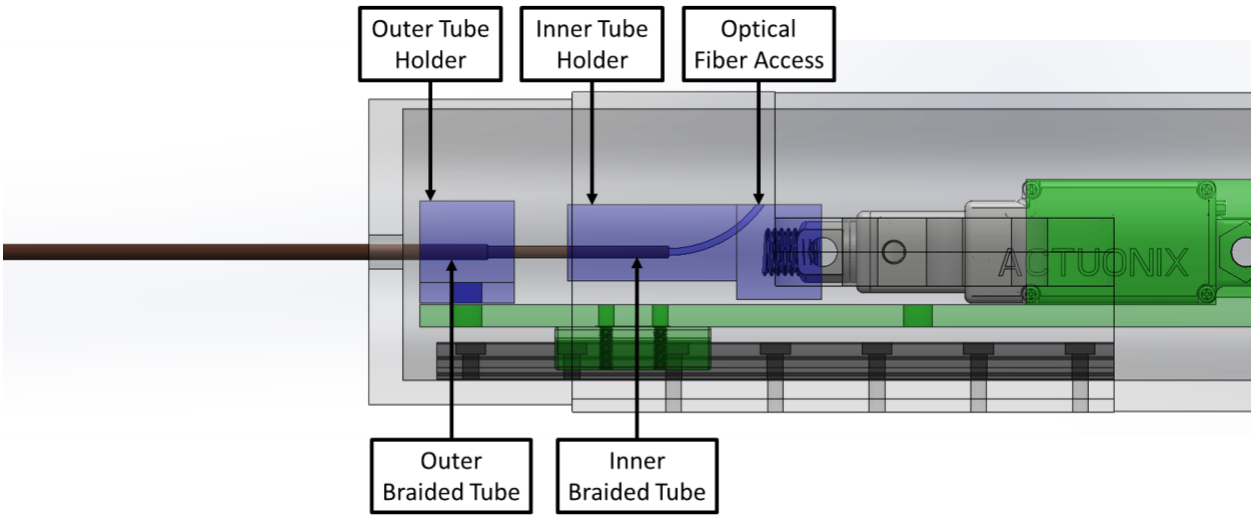


**Figure 2.11**: Cross-sectional view of braided tubes and actuation unit.

### *2.4.2 Heat Shrink*

Traditional endoscopes wrap the camera and the tool together into one larger tube to ensure the two devices stay close to each other and to make their movement more predictable. For the same reasons, we wrapped both sets of braided tubing in a larger tube of medical-grade heat shrink, which acted as an access guide (shown in Figure 2.12). We used heat shrink for the access guide because of its flexibility and its low wall thickness. We used transparent heat shrink with inner diameter 4.75 mm (P/N MT5000-3/16-X-SP, TE Connectivity, Schaffhausen, Switzerland) and length 415 mm.

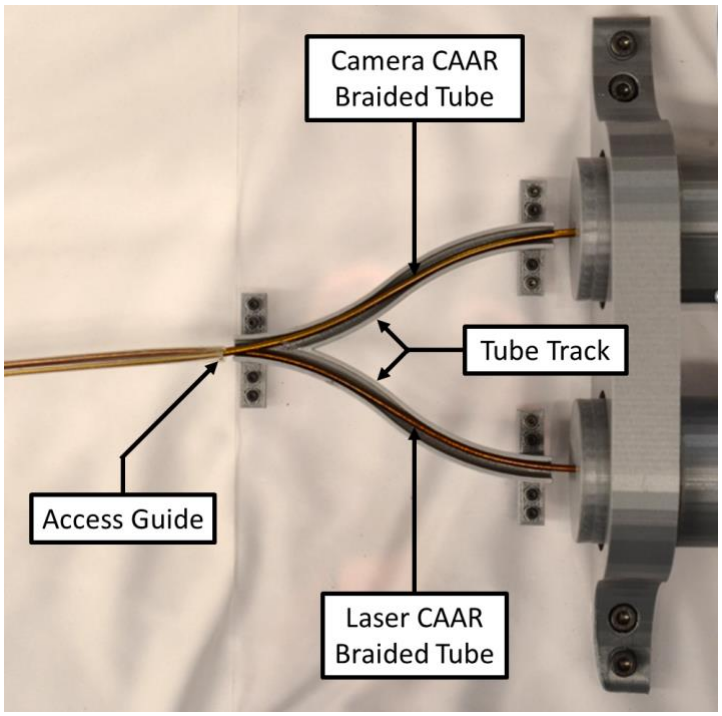


**Figure 2.12**: The tube track brings the two sets of braided tubes together as they exit the actuation unit. The access guide holds the tubes together as they enter the patient.

We brought the two CAARs together as they exited the actuation unit using a tube track, which was designed to guide the two CAARs together such that the braided tubing would bend gradually and would not kink. After assembling the CAARs and attaching them to the actuation unit via the braided tubing, we laid the braided tubes in the tube track and slid the heat shrink over the tubes until the heat shrink reached the tube track. When we inserted the CAARs into the heat shrink, the heat shrink deformed, becoming an ellipse rather than a circle. The ellipse had a major axis of length 5.7 mm and a minor axis of length 4.35 mm. While the access guide did exceed 5 mm in one dimension, its total area of 19.47 $mm^2$ is below that of a traditional endoscope (19.63 $mm^2$).

### 2.5 Actuation Unit

Figure 2.13 displays a rendering of the SCREAM 5 actuation unit. We designed the actuation unit to provide three independent motorized degrees of freedom for both the camera and the optical fiber. We strived to minimize friction in the device to provide the physician with smooth, predictable control over the camera and optical fiber. We prioritized making key components accessible and allowing the physician to easily replace the end effector between procedures. Our design choices led us to create an actuation unit that sits on a platform in front of the patient rather than in the physician's hand; Section 3.6 discusses how the physician controls the new device.

To decouple the three degrees of freedom, we took inspiration from Abell *et al* [9] and Gafford *et al* [10]. These groups designed similar notched-tube continuum surgical robots with three independently actuated degrees of freedom. Figure 2.14 shows that [9] rotated their end effector by encapsulating the components responsible for deflection and translation in the center of a gear; the deflection and translation motors rotate along with the wrist. Figure 2.15 shows that [10] decoupled the end effector's degrees of freedom by nesting their actuation unit components. For example, the winch responsible for deflection is rigidly attached to the lead screw that translates the end effector. As discussed in this section, we nested the sections of our actuation unit as these groups did, so that the translation and rotation motors act equally on both tubes of the CAAR; only the deflection motor causes the tubes to move with respect to each other.

Although we steer the camera and optical fiber using two independent CAARs, the following subsections refer to the actuation of only one CAAR. We actuate both CAARs in the same manner, so the information therein pertains to both CAARs.

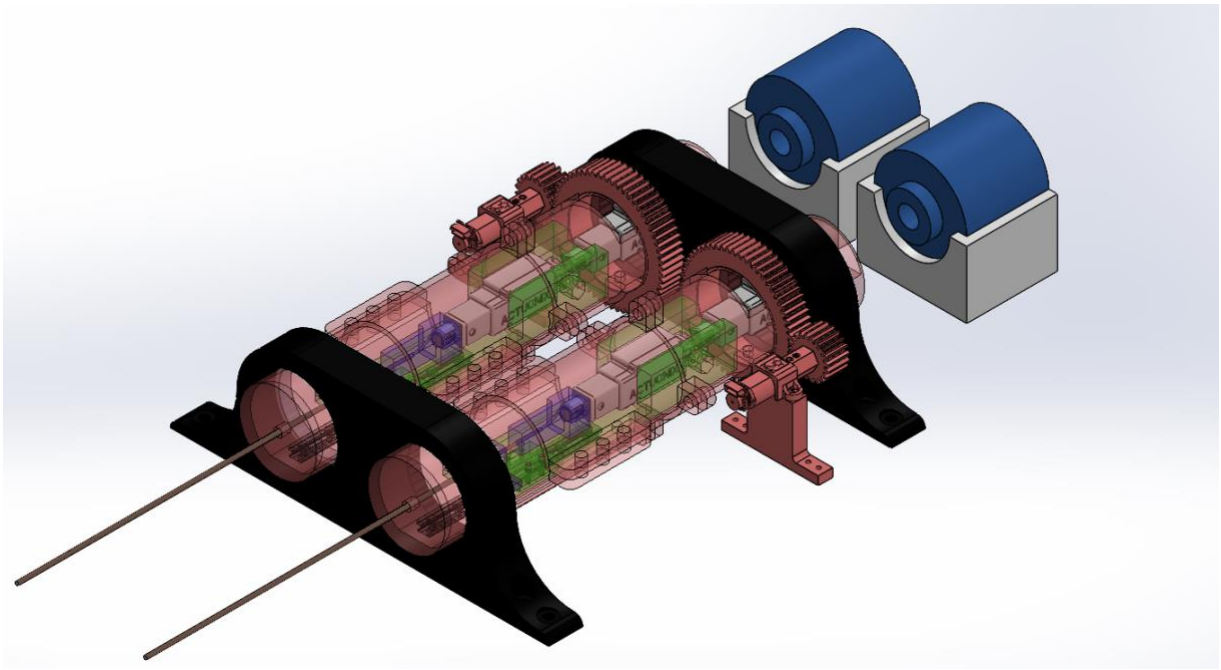

**Figure 2.13**: SCREAM 5 actuation unit. The actuation unit consists of two functionally identical sections: one to control the CAAR that steers the laser fiber and one to control the CAAR that steers the camera. Deflection and translation are achieved using linear ac actuators, which are housed in a cylindrical casing. The casing is supported by bearings at either end, and it has a gear profile on its exterior, which is used to mesh with the motor that achieves rotation. Slip rings at the rear of the actuation unit prevent the wires and surgical instruments from becoming tangled.

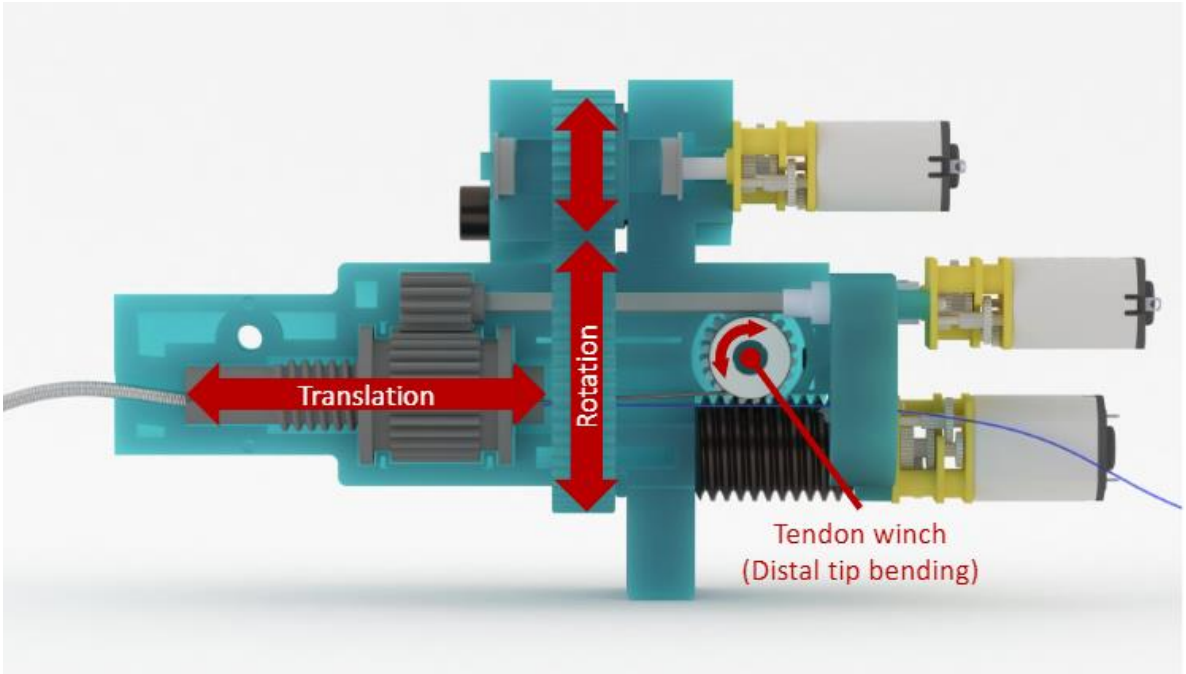


**Figure 2.14**: SCREAM 3 Actuation Unit, with annotations to identify how motion was achieved. Reproduced from [9].

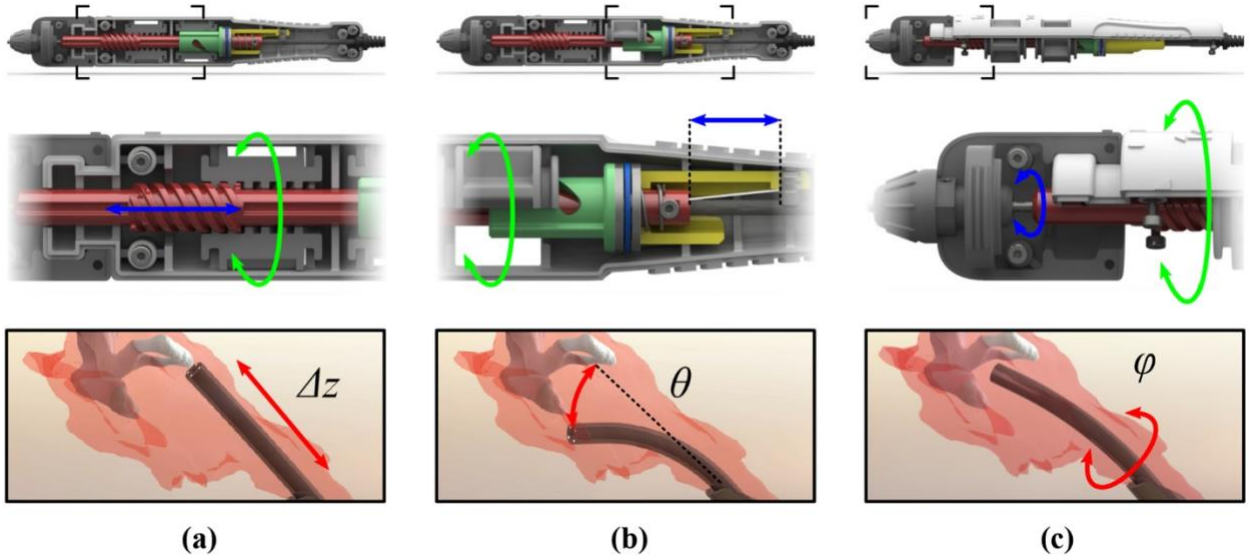


**Figure 2.15**: Endoscope handle that can impose (a) translation, (b) deflection, and (c) rotation in a steerable end effector. Reproduced from [10].

### *2.5.1 Deflection*

Figure 2.16 shows the portion of the actuation unit responsible for deflection and translation of one CAAR. The braided tube connected to the outer section of the CAAR is glued into the outer tube holder, while the braided tube connected to the inner section of the CAAR is glued into the inner tube holder. The end effector (either laser fiber or camera) associated with the CAAR is passed through both holders via the instrument access port. The user achieves deflection by activating the deflection linear actuator; this motor moves the inner tube holder back and forth, causing the inner tube to move while the outer tube remains stationary.

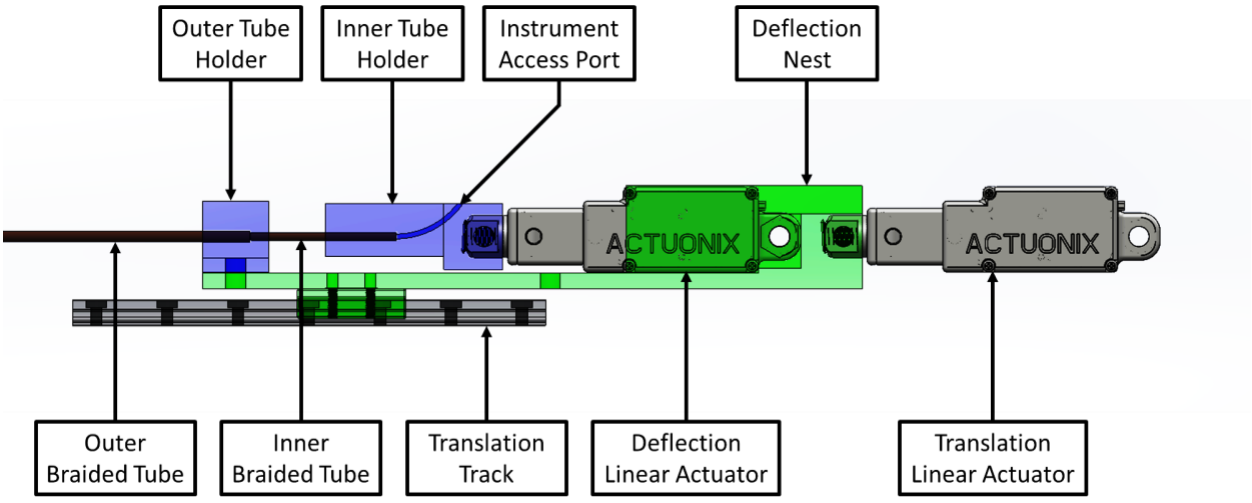


**Figure 2.16**: Side view of the portion of the actuation unit responsible for deflection and translation with important components called out.

We selected the Actuonix L12 linear actuator for this task. Operated at 6 V with a 210:1 reduction, this actuator provides integrated potentiometer feedback, allowing us to measure the actuator's position without purchasing any additional sensors. The actuator has a repeatability of 0.1 mm, and it moves at an easily controllable speed.

### *2.5.2 Translation*

As depicted in Figure 2.16, the Deflection Linear Actuator and the CAAR Outer Tube Holder are rigidly attached to the Deflection Nest. The user achieves translation of the CAAR by activating the Translation Linear Actuator, which moves the Deflection Nest back and forth. Assuming the Deflection Linear Actuator is not also moving, both the inner braided tube and outer braided tube travel together; the CAAR's deflection is therefore unaffected. To support the Deflection Nest and other pieces during translation, we attached the Deflection Nest to a linear carriage, helping to ensure smooth motion and minimal stress on the actuators.

We selected the Actuonix L12 for this task for the same reasons that we selected it for deflection: the integrated potentiometer will help us easily measure the CAAR's position, and the motor's repeatability allows for easy, predictable control.

### *2.5.3 Rotation*

Figure 2.17 shows the deflection and translation components as they are housed in the rotational casing. The rotational casing is a set of three 3D printed pieces that comprise a 245 mm long tube with an outer diameter of 45 mm; one of the pieces also has a 60-tooth gear profile. The user achieves rotation of the CAAR by activating the rotation motor, which is attached to a 20-tooth gear that meshes with the gear on the rotational casing. The components responsible for deflection and translation are rigidly attached to the interior of the rotational casing, so the CAAR rotates with the casing and maintains its current deflection and translation throughout the rotation. Bearings at each end of the rotational casing (shown in Figure 2.13) provide support and allow for smooth motion. Hollow slip rings positioned behind the rotational casing allow the linear actuators inside the casing to rotate without their wires becoming tangled, and they allow the optical fiber and camera wire to pass through unencumbered.

We selected the Pololu Micro Metal Gearmotor LP, powered by 6 V with a 986.41:1 reduction, for this task. Previous SCREAM teams have successfully used this motor for similar applications, and the motor travels at a low speed, allowing for precise control. This motor's free speed is 13 RPM; our gears provide a 3:1 speed reduction, meaning that the rotational casing has a theoretical free speed of 4.33 RPM. This motor is also easily compatible with quadrature encoders, which allow us to track the end effector's rotation.

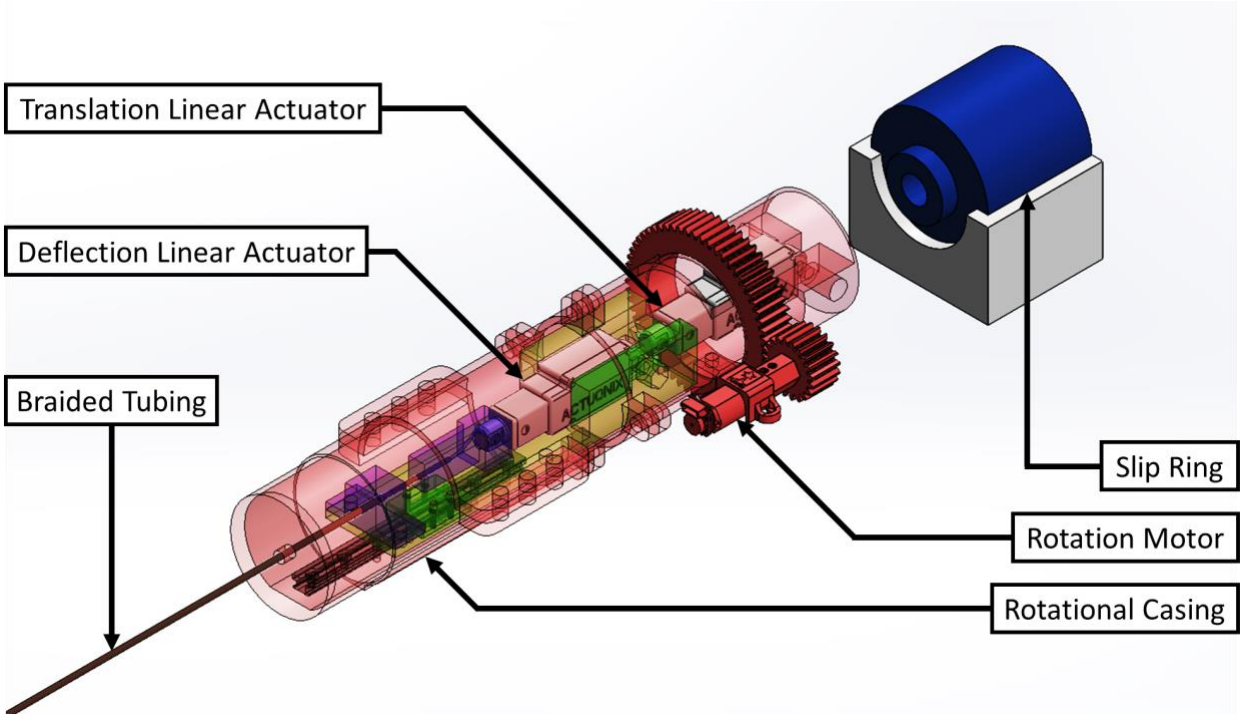


**Figure 2.17**: Portion of actuation unit responsible for the deflection, translation, and rotation of one CAAR. The components required for deflection are housed in the rotational casing. The surgical instrument and the wires that power the linear actuators are passed out the back of the rotational casing and through the slip ring.

## 2.6 Control System

In previous SCREAM projects, the control system was integrated into a handheld endoscope. SCREAM 3 developed a clip-on button panel that allowed physicians to control the endoscope and steerable wrist with one hand. However, the panel orientation in SCREAM 3 was inadequate for effective control, and their system used benchtop power supplies that are not allowed in office surgery settings. SCREAM 4 improved the design by moving the control system off the endoscope to an external unit, eliminating the need for a benchtop power supply. However, its control system lacked intuitiveness for endoscope manipulation. In response to these limitations, we created a control system that will provide physicians with a more intuitive user interface.

The design of our control system was inspired by the Da Vinci SP [16] surgical robot, which consists of several robotic arms controlled remotely by a physician using a display screen, master controls, and foot pedals. By adapting this concept, we eliminated the need for a physician to hold the endoscope during the procedure. Instead, we used a PlayStation 3 (PS3) controller (Sony Interactive Entertainment, San Mateo, California, USA) to offer a comfortable hand placement that avoids awkward finger positions. The controller is operated through Bluetooth to avoid the use of cables. Additionally, the control system is powered by a small voltage supply that is more practical for in-office surgical settings. Figure 2.18 depicts the PS3 controller with annotated control inputs.

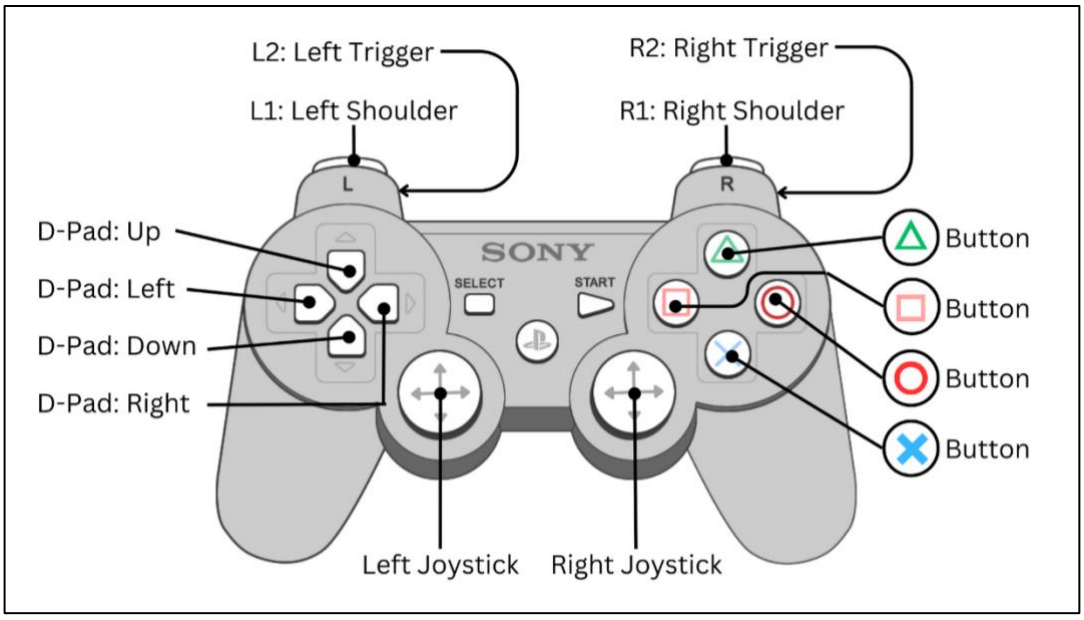


**Figure 2.18**: Diagram of the PS3 Controller used in the SCREAM 5 control system. The controller contains four triggers, eleven buttons, and two two-directional joysticks.

To control the actuators used for deflection and translation, we used the linear actuator with the Actuonix Linear Actuator Control (LAC) board. The LAC is a control board that uses position feedback to accomplish precise control of the linear actuator's position. In our software implementation, we sent PWM signals to the LAC to control the position. The duty cycle of the PWM signal controls the full stroke extension of the linear actuator. A 100% duty cycle fully extends the actuator, while a 0% duty cycle fully retracts.

To control the motors used for rotation, we equipped the motors with quadrature encoders and used the Qunqi L298N Board. The L298N is a dual H-bridge motor driver that can control the speed and direction of two DC motors. We selected the L298N board for its simplicity and its ability to control multiple motors simultaneously. We regulated the motors' speeds using PWM signals to communicate the portion of maximum power that the L298N should provide to the motors.

We used a USB Host Shield, an electronic circuit board that enables communication between a microcontroller board and USB devices, to establish a Bluetooth connection for our system. In our software implementation, we used the corresponding USB Host Shield 2.0 Library [17] to implement the Bluetooth HID protocol for the PS3 controller, allowing the microcontroller board to receive data wirelessly from the controller.

The control system described here required a total of six PWM pins, four interrupt pins, and four digital I/O pins in addition to the pins required by the USB Host Shield. After considering these needs, we selected the Arduino Mega 2560 Rev3 microcontroller, which has a total of 54 digital input/output pins, of which 15 can be used as PWM pins and 6 can be used as interrupt pins.

To satisfy the requirement of SR3, we used a PS3 controller to allow the physician to complete the procedure comfortably. Commonly used in gaming and robotics projects, the PS3 controller is easy to use. We programmed four different control schemes that could be used in the final system (see Figure 2.19). In Method 1, the physician rotates the CAARs using the triggers, translates the CAARs using the buttons, and bends the CAARs using the joysticks. Method 2 uses the triggers to bend, the buttons to rotate, and

the joysticks to translate. Method 3 uses triggers for translation, buttons for bending, and joysticks for rotation. For Method 4, the surgeon must first select the degree of freedom (deflection or translation) they wish to control using the triggers; they then use the buttons to actuate that degree of freedom. Rotation is controlled using the joysticks in Method 4. In all four methods, we split the PS3 controller so that the left side of the PS3 controls the laser CAAR and the right side controls the camera CAAR. This allows the physician to dedicate one hand to each CAAR.

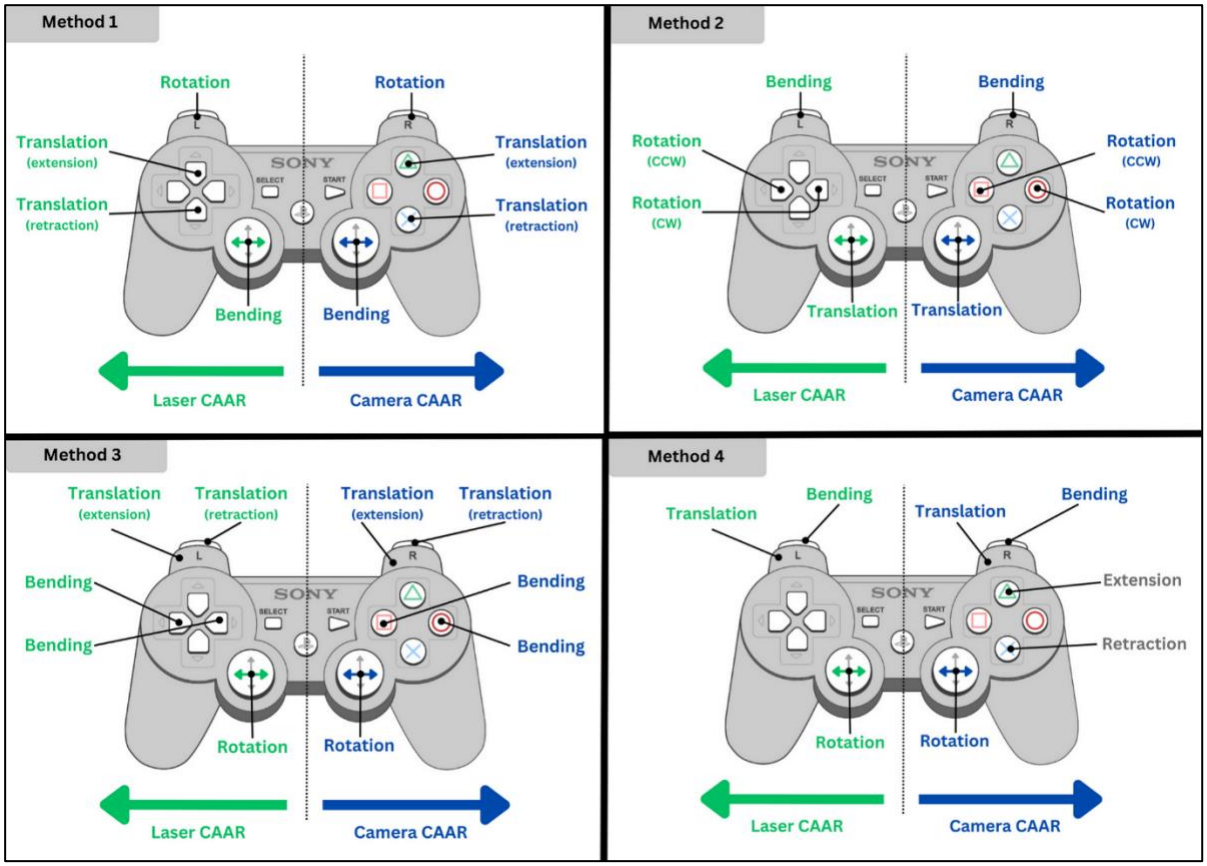


**Figure 2.19**: SCREAM 5 control schemes.

# 3 Experimentation and Validation

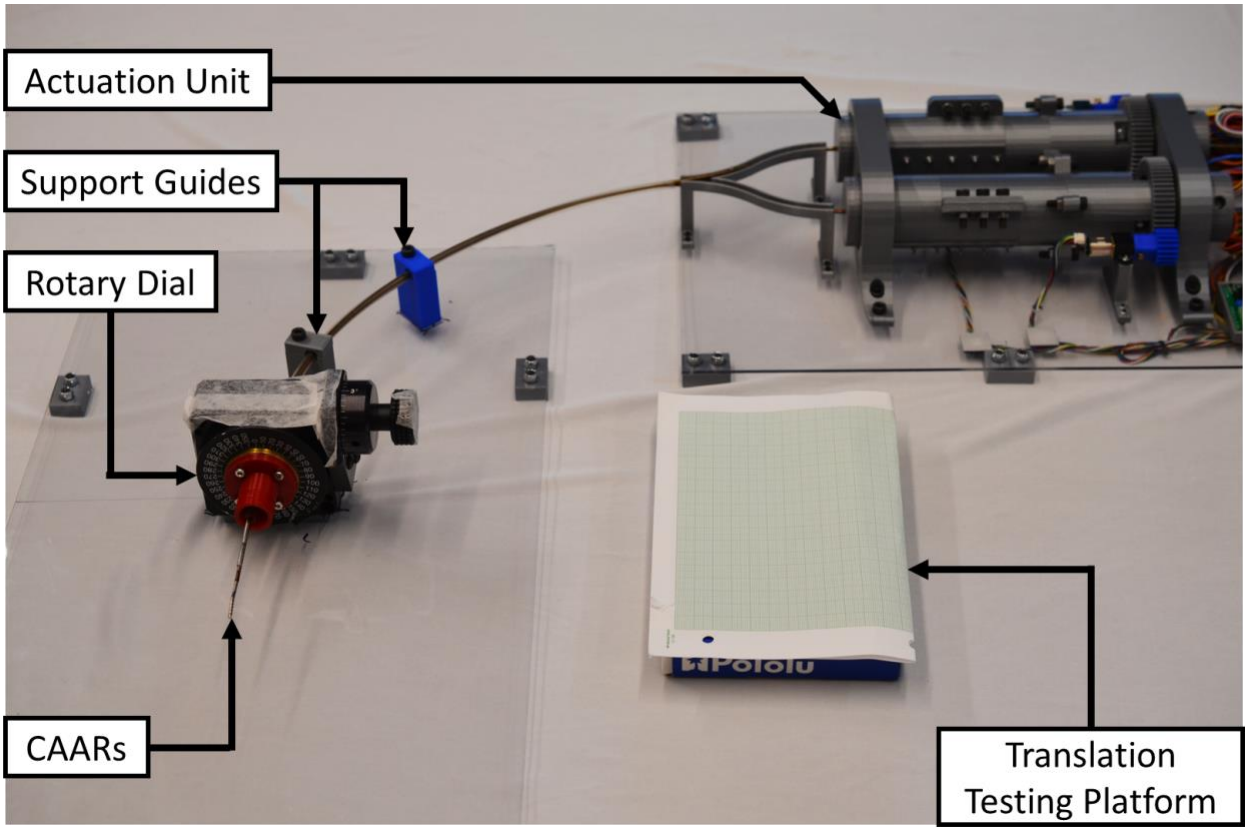


**Figure 3.1**: Fixture used for mechanical validation testing. The translation testing platform was placed directly under the CAARs for the translation portion of the experiment.

We tested the ability of our device to actuate each CAAR using each of the three degrees of freedom: deflection, translation, and rotation. To satisfy SR2, the two CAARs needed to move independently of one another, and motion in one of their degrees of freedom could not affect motion in any of the other degrees of freedom.

## 3.1 Setup

Figure 3.1 depicts the device and the test fixture used for this experiment. The CAARs were attached to the actuation unit using braided tubing. The optical fiber and chip-tip camera were passed through the actuation unit to the distal end of the CAARs. The CAARs were then fed through the rotary dial via the support guides; we executed this experiment with the tube bent approximately 90 degrees to simulate the device being inserted into the larynx.

## 3.2 Deflection

We translated the laser CAAR forward so that the camera CAAR would not interfere with its bending. We then rotated the laser CAAR so that its bending plane would be horizontal. We positioned a digital camera directly above the CAAR to capture images of it throughout the experiment.

Beginning with the deflection linear actuator in its home position (halfway between complete extension and complete retraction), we translated the inner tube of the CAAR forward in increments of 1.0 mm until

the deflection linear actuator was fully extended; we took a picture of the CAAR at each increment. We then returned the CAAR to the home position and translated it in increments of 1.0 mm until the actuator was fully retracted, again photographing the CAAR at each increment.

We repeated this procedure five times for each CAAR. We used a custom MATLAB (MathWorks, Natick, MA, USA) script to analyze the CAAR's bending angle in each picture.

In theory, the displacement of a CAAR's inner tube is related to the CAAR's bending angle according to the following equation [11]:

$$\theta = \theta_0 + \Delta q(\overline{y_1} + \overline{y_2})^{-1}, \tag{3.1}$$

where $\theta_0$ is the angle to which the CAAR was pre-bent, $\Delta q$ is the translation of the inner tube of the CAAR, and $\overline{y_1}$ and $\overline{y_2}$ are the distances from the neutral bending axes of the CAARs' outer and inner tubes, respectively, to the central axis of the CAAR. We did not pre-bend our CAARs, therefore $\theta_0 = 0$. Based on the design parameters discussed in Section 2.3, our steel tubes have neutral bending axes as shown in Table 5.

**Table 55**: Distances of Neutral Bending Axes of CAAR Tubes from Central Axes of CAAR Tubes.

| | Laser CAAR | Camera CAAR |
|---|---|---|
| Inner Tube ($\overline{y_2}$) | 0.5218 mm | 0.8332 mm |
| Outer Tube ($\overline{y_1}$) | 0.8332 mm | 1.0436 mm |

Using Equation 3.1, and the dimensions in Table 3.1, we calculated that the inner tube of the laser CAAR would need to translate 2.13 mm for the CAAR to bend 90° and that the inner tube of the camera CAAR would need to translate 2.95 mm for the CAAR to bend 90°.

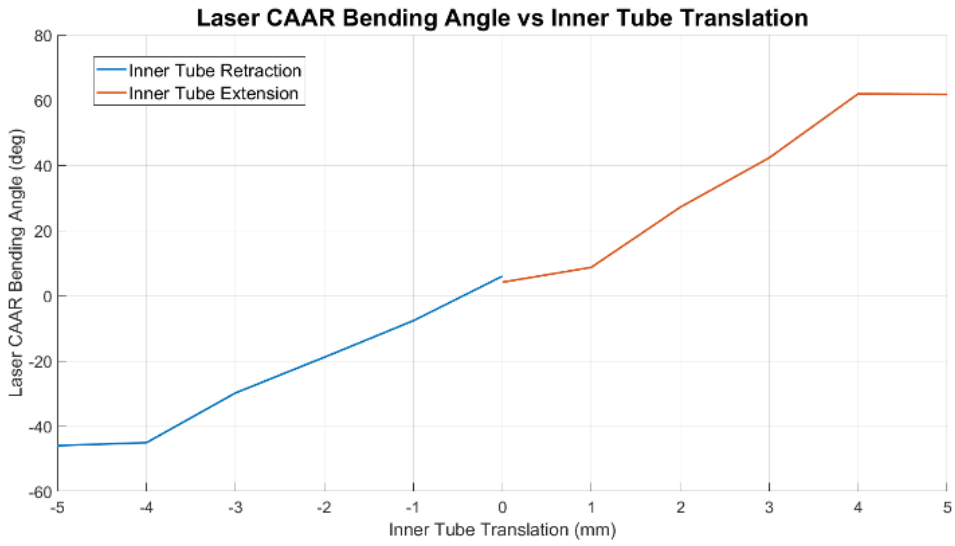


**Figure 3.2**: Relationship between displacement of the inner tube of the laser CAAR and the bending angle of the laser CAAR.

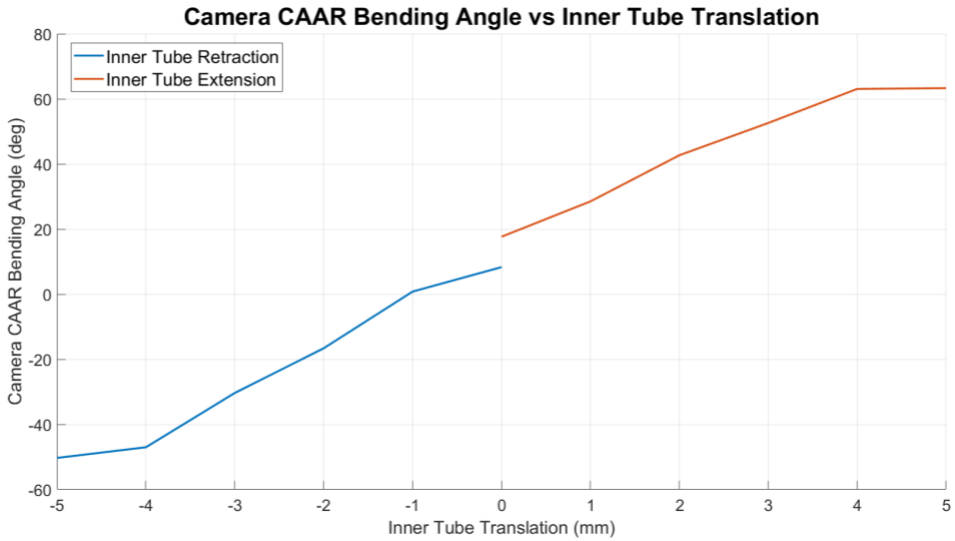


**Figure 3.3**: Relationship between displacement of the inner tube of the camera CAAR and the bending angle of the camera CAAR.

Figures 3.2 and 3.3 display the results of the deflection validation test. After 5 mm of inner tube translation, the laser CAAR reached a maximum deflection of 46.0° in the negative direction and a maximum deflection of 61.9° in the positive direction; the camera CAAR reached a maximum deflection of 50.3° in the negative direction and a maximum deflection of 63.3° in the positive direction.

The relationship between deflection angle and inner tube displacement is linear, as Equation 3.1 suggests. However, the CAARs deflected significantly less than expected. We have identified several factors that contributed to this result. The inner braided tube has some room to shift within the outer braided tube before it transmits forces to the steel tubes; this results in the nonlinearity near 0 mm in Figures 3.2 and 3.3. Additionally, the inner braided tube compresses and tenses when the linear actuator pushes and pulls on it; this means that the braided tube does not transmit forces efficiently and that the translation experienced at one end of the braided tube does not match the translation experienced by the other end. Also, the model proposed in [11] does not account for the friction generated by the tubes rubbing against each other or the kinematic effects of the surgical instrument (laser fiber or camera) passed through the CAAR's center. Finally, the deflection linear actuators could not actuate a full 5 mm in both directions; this causes the nonlinearity around ±5 mm in Figures 3.2 and 3.3.

The standard deviation of bending angle at each increment remained below 7.5° for both CAARs. This demonstrates that our actuation unit provided predictable, repeatable control of the CAARs' deflection.

### 3.3 Translation

To prepare for the translation test, we again positioned a digital camera directly above the CAARs, and we placed 1 cm grid paper under the CAARs. We fully retracted the translation linear actuator for both CAARs and returned the deflection linear actuators to their home positions.

We extended the laser CAAR's translation linear actuator in increments of 1.0 mm until it was fully extended; we photographed the CAAR at each increment. We repeated this process with the deflection

linear actuators at 2.5 mm of extension, 5.0 mm of extension, 2.5 mm of retraction, and 5.0 mm of retraction.

We repeated this procedure five times for each CAAR.

Figures 3.4 and 3.5 display the results of the translation validation test. After 10 mm of input translation, the laser CAAR experienced an output translation of 8.60 mm to 9.05 mm, depending on the CAAR's deflection; the camera CAAR experienced an output translation of 8.50 mm to 9.60 mm, depending on the CAAR's deflection.

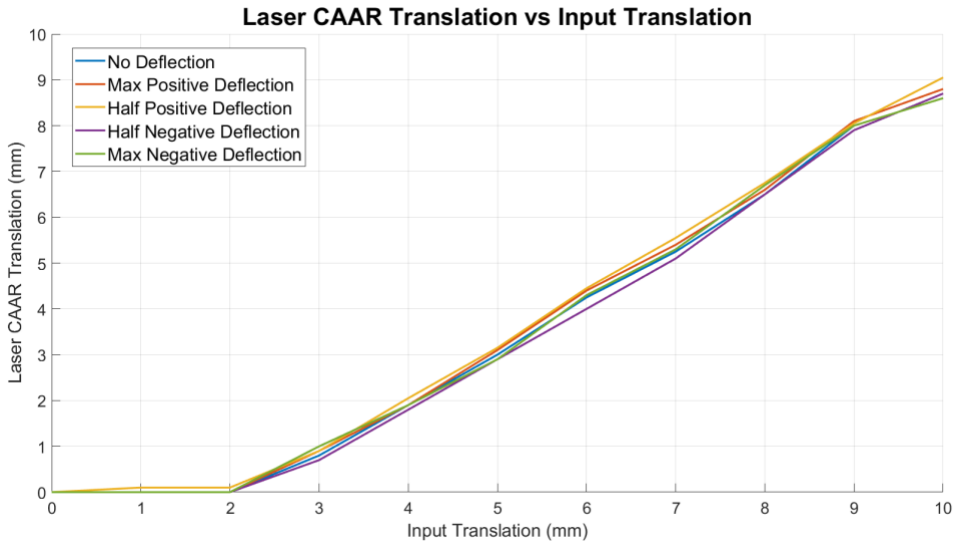


**Figure 3.4**: Relationship between translation input by the actuation unit and translation experienced by the laser CAAR.

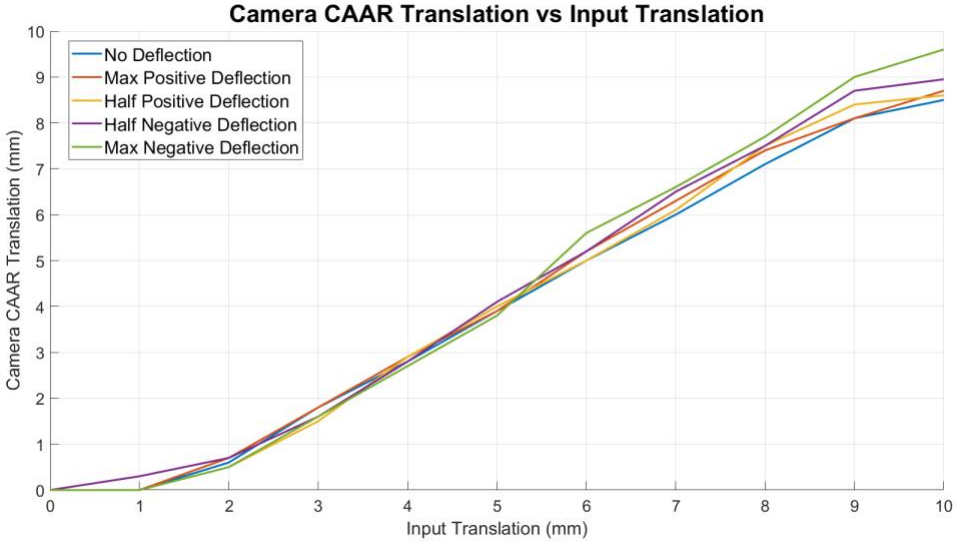


**Figure 3.5**: Relationship between translation input by the actuation unit and translation experienced by the camera CAAR.

The CAARs translated slightly less than the expected 10 mm. Because the braided tubing is not rigidly attached to the tube track or the access guide, it can shift within the access guide, causing the translation of the CAAR to change inadvertently. This extra room in the access guide also causes the dead band at the beginning of Figures 3.4 and 3.5; the braided tubes will shift if possible before they transmit forces to the steel tubes. Additionally, just as in the deflection validation experiment, the linear actuators were unable to reach the full 10 mm of desired translation; purchasing linear actuators with a longer stroke would increase the CAARs' translation range.

The standard deviation in the CAARs' translation did not exceed 0.5 mm at any increment during any trial. This demonstrates that our actuation unit provides predictable, repeatable control of the CAARs' translation.

The CAARs underwent no significant change in bending angle during any of the translation validation trials. This demonstrates the impendence of the translation and deflection degrees of freedom in our device.

### 3.4 Rotation

We again translated the laser CAAR forward so that the camera CAAR would not interfere with its bending. We reset both deflection linear actuators to their home positions. We positioned a digital camera directly in front of the CAAR so that the camera could capture the CAAR's projection onto the rotary dial.

To test the laser CAAR's ability to rotate, we extended the laser CAAR's deflection linear actuator to half of its maximum extension (2.5 mm). We then actuated the rotation motor so that the CAAR would rotate in increments of 30° until either the CAAR had rotated 720° or the wires had become too tangled to rotate further; we photographed the CAAR at each increment. We repeated this test with the deflection linear actuator at full extension, half retraction, and full retraction.

We completed this test five times for the laser CAAR and five times for the camera CAAR.

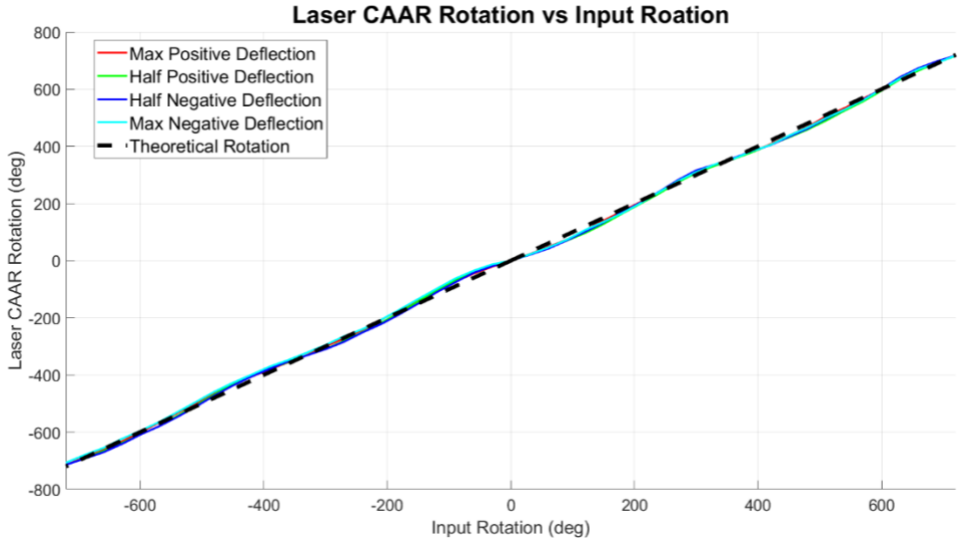


**Figure 3.6**: Relationship between rotation input by the actuation unit and rotation experienced by the laser CAAR.

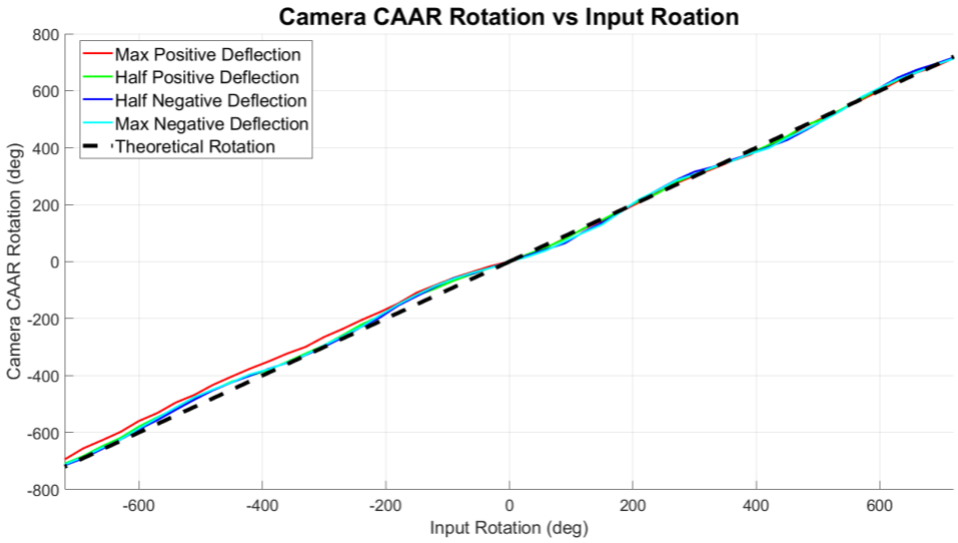


**Figure 3.7**: Relationship between rotation input by the actuation unit and rotation experienced by the camera CAAR.

Figures 3.6 and 3.7 display the results of the rotation validation test. Both CAARs were able to rotate to within 30° of the desired 720° in both directions regardless of deflection. Because we used slip rings to manage the wires and the surgical instruments, we could continue to rotate the CAAR past 720° in either direction; the actuation unit can rotate the CAAR with no limit.

The standard deviation in a CAAR's rotation at any given increment varied significantly, often exceeding 20°. This demonstrates that the actuation unit could not accomplish repeatable position control for CAAR rotation. The variation in rotation angle is a result of the lack of structure in the access guide; restricting the motion of the braided tubes would prevent them from unexpectedly shifting within the access guide and would cause the CAARs' rotation to become more predictable.

# 4 Discussion and Future Work

Our goal for this project was to create a novel surgical robot that allows the physician to perform office-based laser laryngeal surgery. We successfully created a prototype that enables a physician to access previously unreachable areas of the larynx by using a pair of continuum robots. We integrated two CAARs with an actuation unit and wireless controller which allowed the user to control the laser fiber and the camera. The two CAARs were able to be steered independently of each other, each with three degrees of freedom: deflection, translation, and rotation. While we achieved our goal, we have recommendations for how future groups can improve upon our successes.

## 4.1 Future Work

### *4.1.1 Quick Release*

The current design of the robot does not allow for quick and convenient replacement of the steerable sheaths. To replace the sheaths, part of the actuation unit must be taken apart. The next SCREAM team can improve upon our design by adding a quick-release feature to allow the steerable sheaths to be removed from the actuation unit. This would enable the physician to replace the sheaths between procedures without the need for disassembling part of the actuation unit.

### *4.1.2 CAAR Optimization*

The laser and camera CAARs could be optimized for maximum reachability with a minimal diameter. The stainless-steel tubing that was used for this iteration was chosen based upon the diameters of the laser fiber and camera. The CAARs that we used could only bend about 60° in either direction in practice. In a clinical application, the CAAR would need to bend at least 90° in both directions. Future groups could conduct a set of simulations to determine the diameters of tubing and the notch design parameters that allow for maximum reachability. Additionally, the next SCREAM team could incorporate multi-segmented CAARs, rather than the single-segment CAARs that we used this year. A two-segment CAAR would allow greater reachability within the larynx by adding three more degrees of freedom to both the laser fiber and the camera.

### *4.1.3 Laser and Camera She*ath *Material*

Our design used braided tubing to encase the laser fiber and camera as well as to connect the CAARs to the actuation unit. This braided tubing did not transmit force as well as it could have; it often compressed and tensed when it should have been rigid. The compression and tension of the braided tubing negatively affected the reachability of the CAARs. Future teams should research alternative materials that may be more suitable for the sheath material. The ideal material will be rigid enough to not compress or tense when the CAARs are actuated, but also flexible enough to be inserted into the larynx via the nose.

Further work is also necessary to improve the access guide that holds the laser CAAR and camera CAAR together. In our design, we used heat shrink for this purpose. However, we found that the braided tubing was able to shift back and forth inside the heat shrink, which was undesirable. Future groups will need to find an alternative material or design a mechanism that will prevent the shifting of the tubes.

#### *4.1.4 User Study*

In the future, a user study should be done with practicing otolaryngologists to determine if our proposed user interface and control system are reasonable in an office-based surgery setting. We have written a detailed procedure for such a study, which can be found in Appendix C. The next SCREAM team will need to seek IRB approval from Brigham and Women's Hospital to conduct this user study.

#### 4.1.5 *Control System Sophistication*

Future groups could improve upon the control system by adding more sensing capabilities. By detecting when the CAARs crash into each other or into the larynx wall—or by detecting when a crash is imminent—the device could prevent physicians from inadvertently damaging the device and the patient. Additionally, a more thorough visualization could help orient the physician in the larynx by displaying information about the CAARs' global poses. Finally, a haptic control system would allow physicians to feel connected to the device and would inform physicians about the forces experienced by the device.

#### 4.1.6 *Actuation Unit Rotation*

A recurring issue that we encountered while rotating the CAARs was that if one of the CAARs was bent, the other CAAR was unable to rotate a full 360° without colliding with the unbent CAAR. To fix this problem, we propose that the next SCREAM team incorporates a mechanism that allows the entire actuation unit to rotate. Adding a rotating element to the entire actuation unit would add a degree of freedom to the system and would allow the laser fiber and camera CAAR to rotate about each other. This would further improve the physician's ability to navigate the device through a patient's larynx in such a way that the target tumor is visible to the camera and within firing range of the optical fiber.

### 4.2 Conclusion

We successfully created a prototype of a novel surgical robot that would allow a physician to perform laser laryngeal surgery in an office setting. The overall area of the access guide that enters the patient's body is 19.47 $mm^2$. The optical fiber and camera are steered independently using separate concentric agonist-antagonist robots. The optical fiber and the camera each have three degrees of freedom: translation, bending, and rotation. Our CAARs allow the optical fiber to bend to a maximum range of 107.9° at a minimum bending radius of 13 mm and the camera to bend to a maximum range of 113.6° at a minimum bending radius of 16 mm. We can translate the optical fiber up to 9.05 mm, and we can translate the camera up to 9.60 mm. Both the camera and the optical fiber can rotate in both directions without limit. Our device also provides the physician with a wireless control system using a PS3 controller. The final device consists of an independently steered optical fiber and camera, actuation unit, and control unit. Our prototype will hopefully serve as groundwork for future endoscopic devices for in-office laryngeal surgery.

## References


1. J. H. Hah, S. Sim, S.-Y. An, M.-W. Sung, and H. G. Choi, “Evaluation of the prevalence of and factors associated with laryngeal diseases among the general population,” The Laryngoscope, vol. 125, no. 11, pp. 2536–2542, 2015.
2. M. Remacle and H. E. Eckel, Surgery of larynx and trachea. Berlin: Springer, 2010.
3. D. Stoeckel and A. Melzer, “The use of ni-ti alloys for surgical instruments,” Materials in Clinical Applications, ed. by P. Vincenzini. Techna Srl, pp. 791–798, 1995.
4. H. Do, R. Mihaleva, E. Minch, R. Tougas, “SCREAM 4: Super-elastic Continuum Robot for Endoscopic Articulation and Manipulation,” 2022.
5. C. J. Rees, G. N. Postma, and J. A. Koufman, “Cost savings of unsedated office-based laser surgery for laryngeal papillomas,” Annals of Otology, Rhinology & Laryngology, vol. 116, no. 1, pp. 45–48, 2007.
6. C. J. Rees, S. L. Halum, R. C. Wijewickrama, J. A. Koufman, and G. N. Postma, “Patient tolerance of in-office pulsed dye laser treatments to the upper aerodigestive tract,” Otolaryngology–Head and Neck Surgery, vol. 134, no. 6, pp. 1023–1027, 2006.
7. K. O'Brien, C. T. Brolliar, B. G. Mart, and Z. R. Boyer, “SCREAM: Super-elastic Continuum Robot for Endoscopic Articulation and Manipulation,” Digital WPI, 22-Apr-2019. [Online]. Available: https://digital.wpi.edu/concern/student_works/np193c60m?locale=en.
8. J. R. Bartone, N. E. Pacheco, J. F. d'Almeida, and A. J. Gulotta, “SCREAM 2.0: Super-elastic Continuum Robot for Endoscopic Articulation and Manipulation,” Digital WPI, 18-May-2020. [Online]. Available: https://digital.wpi.edu/concern/student_works/g158bk835?locale=en.
9. P. B. Abell, S. Q. Johnson, S. T. Liu, and A. J. Gulotta, “SCREAM 3.0: Super-elastic Continuum Robot for Endoscopic Articulation and Manipulation,” Digital WPI, 27-April-2021. [Online]. Available: https://digital.wpi.edu/concern/student_works/4q77fv16k?locale=en.
10. J. Gafford, M. Freeman, L. Fichera, J. Noble, R. Labadie, and R. J. Webster, “Eyes in ears: A miniature steerable digital endoscope for trans-nasal diagnosis of middle ear disease,” Annals of Biomedical Engineering, vol. 49, no. 1, pp. 219–232, 2020.
11. Kaitlin Oliver-Butler, Zane H. Epps, Daniel Caleb Rucker, "Concentric agonist-antagonist robots for minimally invasive surgeries," Proc. SPIE 10135, Medical Imaging 2017: Image-Guided Procedures, Robotic Interventions, and Modeling, 1013511 (3 March 2017); https://doi.org/10.1117/12.2255549.
12. R. J. Webster and B. A. Jones, “Design and kinematic modeling of Constant Curvature Continuum Robots: A Review,” The International Journal of Robotics Research, vol. 29, no. 13, pp. 1661–1683, 2010.
13. I. A. Chan, J. F. d'Almeida, A. Chiluisa, T. L. Carroll, Y. Liu, and L. Fichera, “On the merits of using angled fiber tips in office-based laser surgery of the vocal folds,” Medical Imaging 2021: Image-Guided Procedures, Robotic Interventions, and Modeling, 2021.
14. P. Cignoni, M. Callieri, M. Corsini, M. Dellepiane, F. Ganovelli, and G. Ranzuglia, “Eurographics Italian Chapter Conference,” in MeshLab: an Open-Source Mesh Processing Tool, 2008, pp. 129–136.
15. M. M. Hess, “KTP laser in the Office,” ENT & Audiology News, 01-Mar-2016. [Online]. Available: https://www.entandaudiologynews.com/development/how-i-do-it/post/ktp-laser-in-the-office.
16. “Robotic-Assisted Surgery with da Vinci Systems,” Intuitive.com. [Online]. Available: https://www.intuitive.com/en-us/patients/da-vinci-robotic-surgery.
17. O. Mazurov, “USB Host Library Rev. 2.0,” GitHub, May 30, 2022. https://github.com/felis/USB_Host_Shield_2.0.
18. J. Suárez-Quintanilla, A. F. Cabrera, and S. Sharma, “Anatomy, head and neck: Larynx,” StatPearls, 05-Sep-2022. [Online]. Available: https://www.statpearls.com/articlelibrary/viewarticle/24061/.
19. K. M. Lynch and F. C. Park, Modern Robotics: Mechanics, planning, and Control. Cambridge, MA: University Press, 2021.

20. E. K. DeVore, A. J. Chiluisa, E. V. Minch, R. Mihaleva, H. Do, R. Tougas, L. Fichera, and T. L. Carroll, “Benefits of side-firing optical fibers in endoscopic laser treatment of the larynx,” The Laryngoscope, vol. 133, no. 5, pp. 1205–1210, 2022.
21. H.-C. Hu, S.-Y. Lin, Y.-T. Hung, and S.-Y. Chang, “Feasibility and associated limitations of office-based laryngeal surgery using carbon dioxide lasers,” JAMA Otolaryngology–Head & Neck Surgery, vol. 143, no. 5, pp. 485–491, 2017.
22. P. J. Swaney, P. A. York, H. B. Gilbert, J. Burgner-Kahrs, and R. J. Webster, “Design, fabrication, and testing of a needle-sized wrist for surgical instruments,” Journal of Medical Devices, vol. 11, Dec. 2016.
23. “StateSpace,” Create an RRT planner for geometric planning - MATLAB. [Online]. Available: https://www.mathworks.com/help/nav/ref/plannerrrt.html.
24. Bailly, T. Cochereau, L. Orgeas, N. H. Bernardoni, S. R. Du Roscoat, A. Mcleer-Florin, Y. Robert, X. Laval, T. Laurencin, P. Chaffanjon, et al., “3d multiscale imaging of human vocal folds using synchrotron x-ray microtomography in phase retrieval mode,” Scientific reports 8(1), 2018.

## Appendix A: Manufacturing Process for the Laser and Camera CAARs

### Materials

To fabricate the notched tubes for the laser and camera CAARs, we used the following materials:

- 0.095” diameter stainless steel tubing
- 0.078” diameter stainless steel tubing
- 0.05” diameter stainless steel tubing
- 1 mm diameter carbide square-end two flute end mill TiCN coated
- 0.05” diameter uncoated carbide square end mill 4 flute
- 5/64” diameter uncoated carbide square end mill 4 flute
- 1.25” x 1.25” x 2” aluminum block
- Loctite super glue

### Machine and Tooling

We used a Haas Standard Mini Mill (Oxnard, CA, USA) to machine the laser and camera CAARs. To cut the stainless-steel tubing, we used a 1 mm diameter carbide square end two flute TiCN-coated endmill. Because of the hardness of the stainless-steel tubing, a coated endmill allowed for less deflection in the endmill as compared to an uncoated endmill. The 0.05” and 5/64” diameter endmills were used to mill the fixtures.

### CAM

The first step in the machining process was to create the computer-aided machining (CAM) file. For this project, we used ESPRIT CAM. Because of the shape of the fixture and the stainless-steel tubing, it was easier to draw the basic geometry of the cuts rather than import a CAD file.

### Feeds and Speeds

The feeds and speeds were carefully chosen for this process, as the hardness of the stainless-steel and the small diameter of the endmill could cause significant deflection in the endmill. The program G-Wizard was used to calculate the feeds and speeds and to gauge the amount of deflection that the endmill would undergo. The cut speed, 6,000 revolutions per minute, was a fixed value, as the mill had a maximum spindle speed of 6,000 revolutions per minute. The feeds and speeds used to cut both CAARs can be seen in Table 6.

**Table 6**: Feeds and speeds for machining the laser and camera CAARs.

| | Laser | Camera |
|---|---|---|
| **Cut Speed (RPM)** | 6000 | 6000 |
| **XY Feed Rate (IPM)** | 2.400 | 2.500 |
| **Z Feed Rate (IPM)** | 2.546 | 2.500 |

### Fixturing

Due to the unique shape of the part, we had to make a fixture to hold the tubing during the machining process. This fixture was made by cutting a slot in a 1.25” x 1.25” x 2” aluminum block. The width of the slot was equal to the diameter of the tubing. The height of the slot was equal to half of the diameter of the tubing. The stainless-steel tubing was then fixed to the aluminum block using Loctite super glue.

**Finished Part Release**

To release the part from the fixture, we used acetone to dissolve the glue. We allowed the fixture and the machined part to sit, fully submerged, in a bath of acetone for ten minutes before separating the tubing from the fixture.

## Appendix B: Manufacturing Process for the Laser and Camera Endcaps

### Materials

To fabricate the laser and camera endcaps, we used the following materials:

- 1/16” drill bit
- 0.0125” drill bit
- 1/32” spot drill
- 1 mm diameter carbide square-end two flute end mill TiCN coated
- 0.05” aluminum sheet
- 3” x 2” x 1.25” aluminum block
- Loctite super glue
- Painter’s tape

### Machine and Tooling

We used a Haas Super Mini Mill (Oxnard, CA, USA) to manufacture the laser and camera endcaps. We chose this machine because it has a maximum spindle speed of 15,000 revolutions per minute. Having a higher spindle speed than a standard mini mill, which has a spindle speed of 6,000 revolutions per minute, was advantageous for this process because of the small diameter of the endmill and drill bits.

### CAM

A CAD model was used to aid in the machining process of the endcaps. The model can be seen below in Figure A.5. This CAD model was imported into ESPRIT CAM, where the machining process was created. During this process, both the laser and camera endcaps were made at the same time.

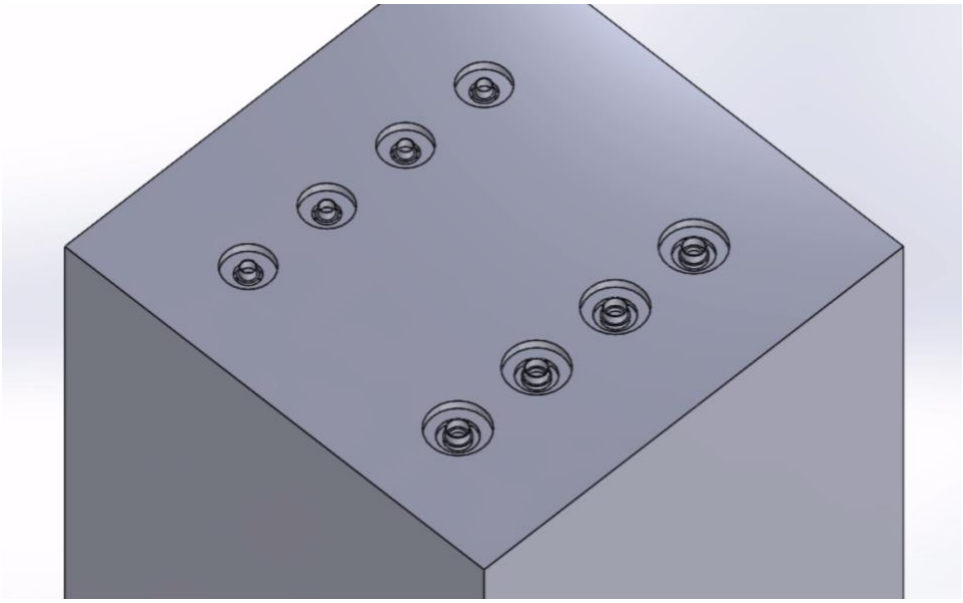

**Figure B.1**: CAD model of four laser endcaps and four camera endcaps.

**Feeds and Speeds**

The feeds and speeds for the endcaps machining process were calculated using the program G-Wizard. The cut speed, 15,000 rpm, was a fixed value, as the mill had a maximum spindle speed of 15,000 revolutions per minute. The feeds and speeds for the milling and drilling operations used in this process are shown in Table 7.

**Table 7**: Feeds and speeds for endcap machining and drilling operations.

| | Milling | Drilling |
|---|---|---|
| **Cut Speed (RPM)** | 15000 | 15000 |
| **XY Feed Rate (PM)** | 9.000 | 9.000 |
| **Z Feed Rate (PM)** | 4.000 | N/A |

**Fixturing**

To manufacture the endcaps, a fixture was used to hold the aluminum sheet. A 3” x 2” x 1.25” aluminum block was used as a base. A piece of painter’s tape was placed over the block. The tape was used as a method to easily remove the endcaps from the fixture. The aluminum sheet was then glued to the tape using Loctite super glue.

**During Machining**

During the machining process for the endcaps, it is important to not use any coolant at all. The surface area between the fixture and the endcaps is minimal, and the glue between these two surfaces will not be able to withstand the coolant flow. The lack of coolant during this process did not affect the surface finish of the machined parts in any significant way.

## Appendix C: Physician User Study

The purpose of this user study is to find the best way for physicians to control our surgical device during laryngeal procedures. We created four control methods using a PS3 controller as an input device (see Figure 3.14). The following text describes the proposed user study.

To enlist participants for the study, the team should contact the project's clinical advisor, Dr. Thomas Carroll. In consultation with Dr. Carroll, the team should assemble a set of otolaryngologists with experience performing endoscopic laser surgery. These surgical experts will be able to provide expert insight about how physicians may respond to our proposed device as well as what physicians would desire in such a device.

To replicate the conditions of a real laryngeal procedure, participants will be standing in front of a computer monitor displaying the camera CAAR within the larynx mold. The surgical device and the larynx model will be positioned away from the participant and monitor.

During the user study, participants will be tested on all four control methods. Using each control method, they will need to fire the laser at three different target points (each in a different larynx model). During the trials, participants will be asked to stand behind the monitor and use the wireless controller to guide the device into the larynx model, find the marker using the camera, and fire the laser CAAR at the marker. Once they have fired the laser, they will be given another larynx model with a different location marker. They will repeat this process until the participants have completed all three tasks.

The study will last for four consecutive days, and each day will be devoted to testing one of the four control methods. In total, each participant will undergo 12 trials, with three trials for each control method. To prevent bias, the order of the control methods will be randomized across participants. All participants will be instructed to stand throughout the experiment, as long as they are physically able to do so.

The following procedure describes the sequence of events associated with the user study:

1. Introduction: Participants will be introduced to the device developed by the research team and informed about the purpose and nature of the user study.
2. Pre-Survey: Prior to beginning the trials, participants will complete a pre-survey to determine their baseline experience with a PS3 controller (see below).
3. Control Method Overview: After completing the pre-survey, participants will receive a brief overview of the control method they will be tested on that day.
4. Familiarization Period: Participants will have two minutes to familiarize themselves with the controls without using the larynx model and without any knowledge of the trials.
5. Trial Introduction: Once the familiarization period is over, participants will be introduced to the trials.
6. Practice Session: Participants will be shown the larynx model and given one minute to practice moving the CAARs in the larynx model.
7. Trial Execution: For each of the three larynx models, participants are given a maximum of two minutes in which they will have to navigate to and fire the laser upon the location of the taped marker.
8. Post Trial Survey: Participants will be given the trial post survey where they will be asked to rate their experiences on a Likert scale (see below).

9. Repeat Trials: Repeat steps 3-8 until the participant has completed all four control method tests.
10. Overall Post Survey: At the end of the fourth day of the user study, participants will complete an overall post-survey to provide their final feedback on the study (see below).

Both qualitative and quantitative metrics will be used to evaluate the performance of participants during the trials. The team will measure the distance between the taped marker and the location where the participant fired the laser. The team will measure the amount of time (capped at 120 seconds) that the participant took to fire the laser, as well as the amount of time the participant used to practice before completing the trials. The team will gather feedback from the post-surveys to gauge participants' opinions of the control methods.

**Pre Survey**

This survey is to be taken at the beginning of the user study before the participant has been introduced to the surgical device or the control system.

1. Please rate your experience level using a PlayStation 3 controller on a scale from 1 (never used it before) to 5 (used very frequently).
2. How many years of experience do you have performing endoscopic laryngeal operations?

**Trial Post Survey**

This survey is to be taken immediately after the user completes a trial using one of the four proposed control methods.

1. Which method did you complete today? (Method 1, Method 2, Method 3, or Method 4)?
2. On a scale from 1 (impossible) to 10 (no difficulty whatsoever), how easy was it to use the controller to complete the task?
3. On a scale from 1 (impossible) to 10 (no difficulty whatsoever), how did the triggers correspond with their respective degree(s) of freedom?
4. On a scale from 1 (impossible) to 10 (no difficulty whatsoever), how did the buttons correspond with their respective degree(s) of freedom?
5. On a scale from 1 (impossible) to 10 (no difficulty whatsoever), how did the joysticks correspond with their respective degree(s) of freedom?

**Overall Post Survey**

This survey is to be taken after the participant has completed all four methods.

1. Of the four control methods, which did you prefer overall?
2. Please explain your answer to the previous question.
3. Which control method did you find hardest to use?
4. Please explain your answer to the previous question.
5. Please rank the control methods based on how intuitive you find them.
6. Based on your experience using the different control methods in this study, do you think there might be a different arrangement of control inputs that would allow a physician to more intuitively control a robot's movements? If so, please describe the combination you think would work better.
7. Are there any additional features or control options that you would like to see added to this control system? If so, please elaborate.

## Appendix D: Control System Wiring Schematic

Figure D.1 shows how we create the 6 V power line that we use to power the motors. Each of these voltage regulators steps a 12 V input down to a 6 V output. To reduce the load on the regulation circuit and to ensure that we do not draw too much current from a single regulator, we use three regulators: one to power the two deflection actuators, one to power the two translation actuators, and one to power the two rotation motors.

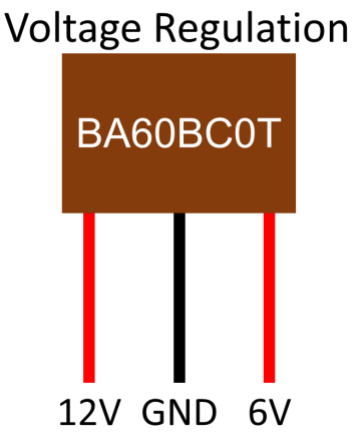


**Figure D.1**: Voltage regulation circuit.

Figure D.2 shows how we control the deflection and translation of a CAAR. We power the LACs with the 6 V that is output by the voltage regulation circuit, and we communicate the desired motor position to the LAC via a PWM signal. Because the microcontroller operates at a 5 V logic level and the LAC operates at a 3.3 V logic level, we use a voltage divider to step down the PWM signal's voltage level. The LACs use the PWM signal and the linear actuators' potentiometer feedback to move the actuators to the desired positions. The slip ring allows the actuators to rotate without their wires tangling.

Figure D.3 shows how we control the rotation of the CAARs. We power the L298N motor controller, which can independently control two motors, with the 6 V that is output from the voltage regulation circuit. To control the direction of each motor, we set one of the motor's inputs (IN1 and IN2 for the laser CAAR, and IN3 and IN4 for the camera CAAR) to 5 V and the other to 0 V. To control the motor's speed, we transmit a PWM signal to the motor's corresponding EN pin. To measure the motor's position, we connect the two encoder signal wires to interrupt pins on the microcontroller, which also provides the 5 V line used to power the encoders.

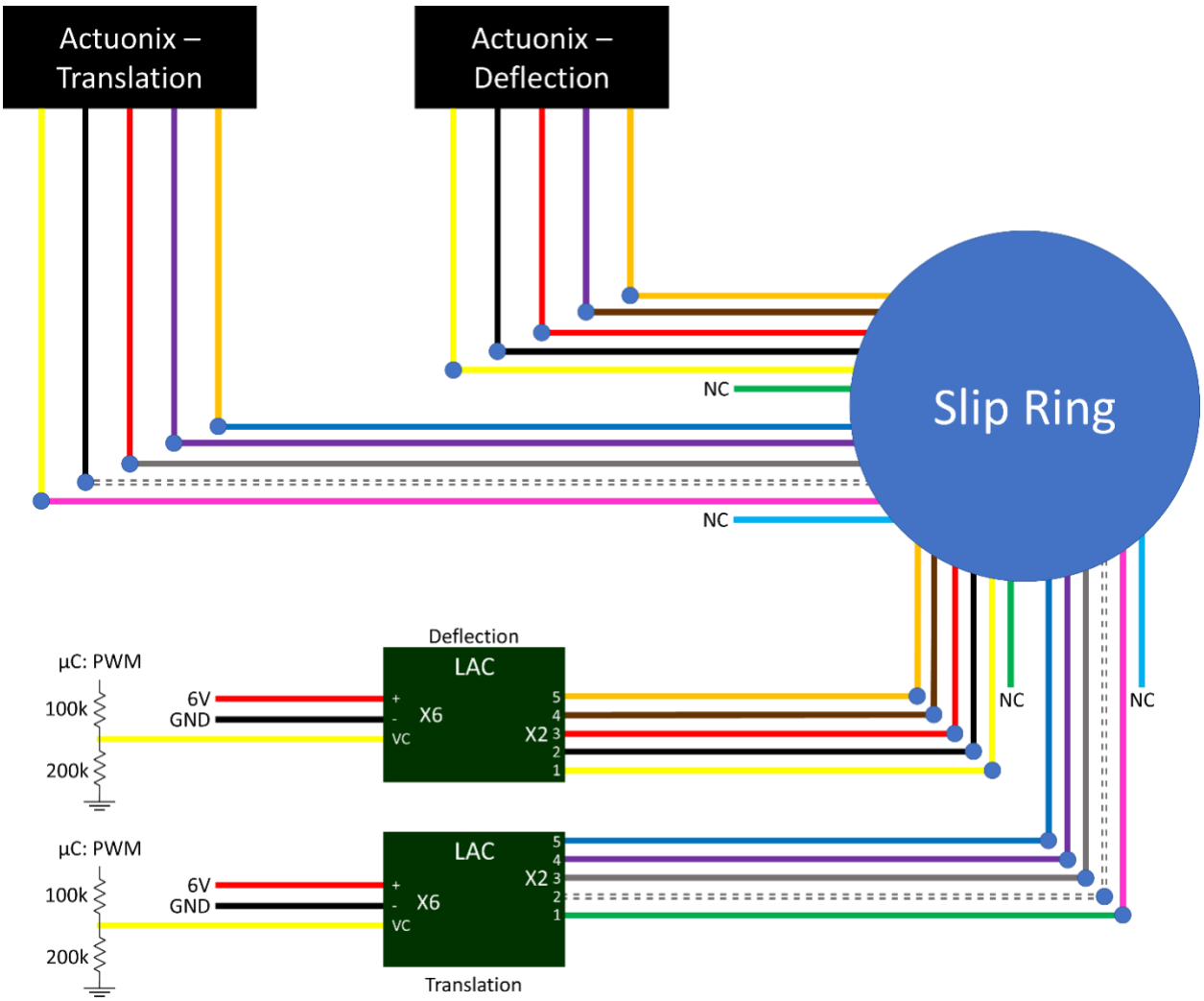


**Figure D.2**: Circuitry to control deflection and translation of one CAAR.

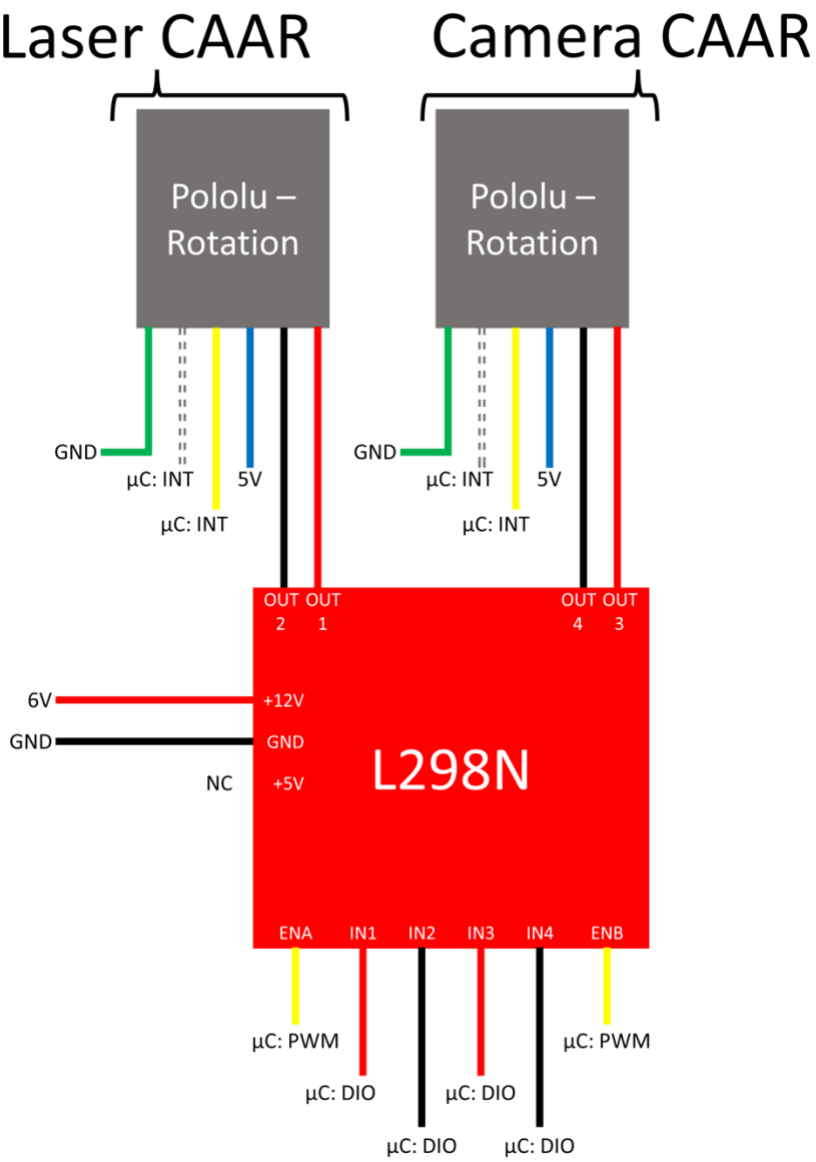


**Figure D.3**: Circuitry to control the rotation of both CAARs.